

Dimensionality Reduction for Remote Sensing Data Analysis: A Systematic Review of Methods and Applications

Nathan Mankovich, Kai-Hendrik Cohrs, Homer Durand,
Vasileios Sitokonstantinou, Tristan Williams, and Gustau Camps-Valls
*Image Processing Lab, Universitat de València, C/ Cat. Agustín Escardino Benlloch,
9, Paterna, 46980, València, Spain*

Abstract

Earth observation involves collecting, analyzing, and processing an ever-growing mass of data. This planetary data is crucial for addressing relevant societal, economic, and environmental challenges, ranging from environmental monitoring to urban planning and disaster management. However, its high dimensionality entails significant feature redundancy and computational overhead limiting the effectiveness of machine learning models. Dimensionality reduction (DR) techniques, specifically feature extraction, address these challenges by preserving essential data properties while reducing redundancy and enhancing tasks in Remote Sensing (RS). The landscape of DR for RS is a diverse, disorganized, and rapidly evolving field. We offer a practical guide for this landscape by introducing a framework of DR. Using this framework, we trace the evolution of DR across the data value chain in RS. Finally, we synthesize these trends and offer perspectives for the future of DR in RS by first characterizing this shift from single-task models to unified representations, then identifying two perspectives in the foundation model era: the need for robust and interpretable DR and the potential of bridging classical DR with modern representation learning.

Keywords: Dimensionality reduction, Remote sensing, Foundation model, Principal component analysis, Manifold learning

1. Introduction

Advancements in Remote Sensing (RS) technologies have ushered in an era of unprecedented data availability, with modern RS platforms continuously generating high-resolution spatial, spectral, and temporal Earth observation data from local to global scales. Data volume, velocity, variety, and dimensionality are expected to grow faster as imaging systems improve [145]. These datasets have revolutionized domains such as environmental monitoring [99], natural resource management [89], urban planning [194], agricultural activity monitoring [193], and disaster management [178], offering essential information to support timely and informed decision-making.

The fact is that sophisticated data processing techniques are crucial for extracting actionable insights from complex datasets. These methods, including data mining and machine learning, help identify patterns, make predictions, and derive meaningful interpretations. However, high data volume and dimensionality—across spectrum, space, and time—present significant challenges. For example, satellites like the Sentinel missions produce 8 to 12 terabytes of synthetic aperture radar (SAR) and optical imagery daily [161], and the near-real-time data stream from weather satellites such as the geostationary operational environmental satellite (GOES-R) series provides continuous monitoring of atmospheric conditions [60]. Furthermore, the volume, variety, and complexity of RS data dimensionality are illustrated in Fig. 1. As dimensions increase, many techniques become computationally impractical. Even with large datasets, high dimensionality can lead to unreliable distance metrics and an increased risk of overfitting in machine learning models. These problems are commonly summarized as *the curse of dimensionality* [4].

To address these issues and fully extract value from the data, dimensionality reduction (DR) methods play a crucial role. DR methods are primarily divided into those that select relevant features and those that optimally extract them. Unlike feature selection techniques, DR for feature extraction analyzes the original data and *extracts low-dimensional features* from high-dimensional data while preserving the essential properties needed for downstream analysis. DR methods to extract low-dimensional spectral, spatial, and/or temporal features can enhance the value of RS data from preprocessing and analysis to the improvement of RS products. Over the last century, the field of DR has grown in popularity and developed a dense, fragmented landscape of DR methods, ranging from linear multivariate analysis to deep learning (see Fig. 2). Thus, the problem of high-dimensional data can be

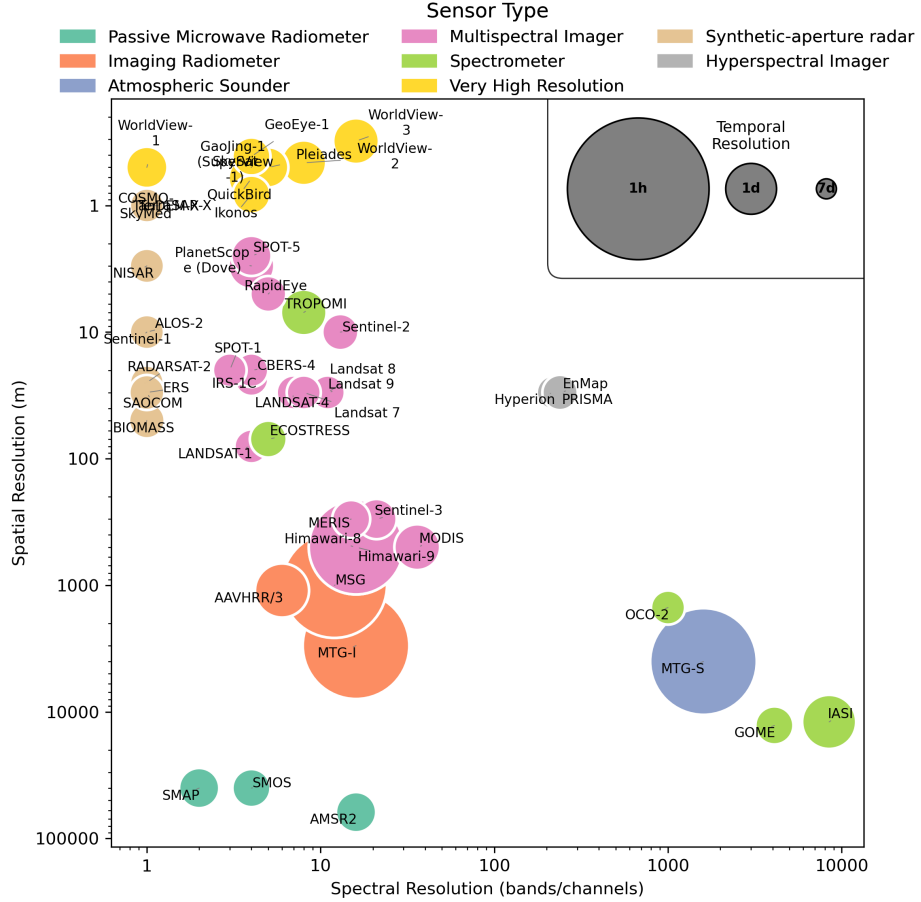


Figure 1: **The utility of DR for RS data from various widely used Earth observation sensors.** We show a simplified representation of the dimensions of remote sensing data, with spectral on the x-axis, spatial on the y-axis, and temporal indicated by the circle size. In the legend, any circle larger than the left circle has a revisit time exceeding an hour, and any circle smaller than the right circle has a revisit time less than weekly. Of course, many other dimensions in these data introduce redundancy (see Tab. A.4). Airborne instruments (e.g., AVIRIS, HyMap, UAVSAR, and airborne LiDAR) share the same sensing modalities as their spaceborne counterparts but differ in spatial scale, revisit pattern, and acquisition flexibility.

addressed by a DR method, but it is replaced by a secondary problem of selecting the optimal method from the vast DR landscape.

With the proper navigation tools for the DR landscape, families of methods can be identified for specific RS tasks at each level of the RS data value

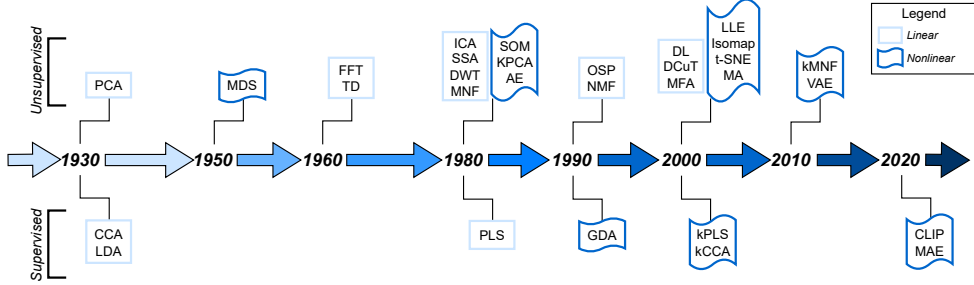


Figure 2: **A timeline of common DR methods.** DR for feature extraction began with linear multivariate analysis methods like Principal Component Analysis (PCA) [72] in the 1930s, and became popular in the RS community in the 1970s [116]. The nonlinear DR boom began in the late 1900s, including manifold learning and methods such as kernel PCA (kPCA) [153], and was quickly adopted by the remote sensing community within 10 years [23]. Increasing computing power has enabled the popularity of deep learning-based DR methods, such as the Variational Autoencoder (VAE) [88]. Deep learning has been quickly adopted by the RS community [211]. This paved the way for modern deep learning methods, like Contrastive Language-Image Pre-training (CLIP) and Masked Autoencoders (MAE). These methods are already being applied in RS (e.g., Sat-CLIP [90]). See Tab A.5 for a glossary of DR abbreviations.

chain. Previous works navigate the landscape of DR with an eye for RS applications by either focusing on hyperspectral data [144, 134], specific RS data tasks [46, 143, 98, 41, 73, 124], or by restricting to small pieces of the DR landscape [134, 186, 78]. For example, some taxonomies only address linear methods [177] or overlook them entirely [95]. Meanwhile, others miss a perspective on deep learning [129].

We address all three limitations through a modern, comprehensive review of DR methods applied across the entire RS data value chain, one that moves beyond hyperspectral data analysis and incorporates the transition in modern DR, moving towards deep learning and foundation models. What follows is a guide for using DR in RS, outlined in Fig. 3. This guide begins with a framework of standard DR methods in RS. Using this framework as a map, we provide a systematic survey of DR applications for improving each task in the RS data value chain and outline standard metrics for DR evaluation in RS. Finally, we summarize the trends and perspectives, outlining the way forward for DR in RS applications.

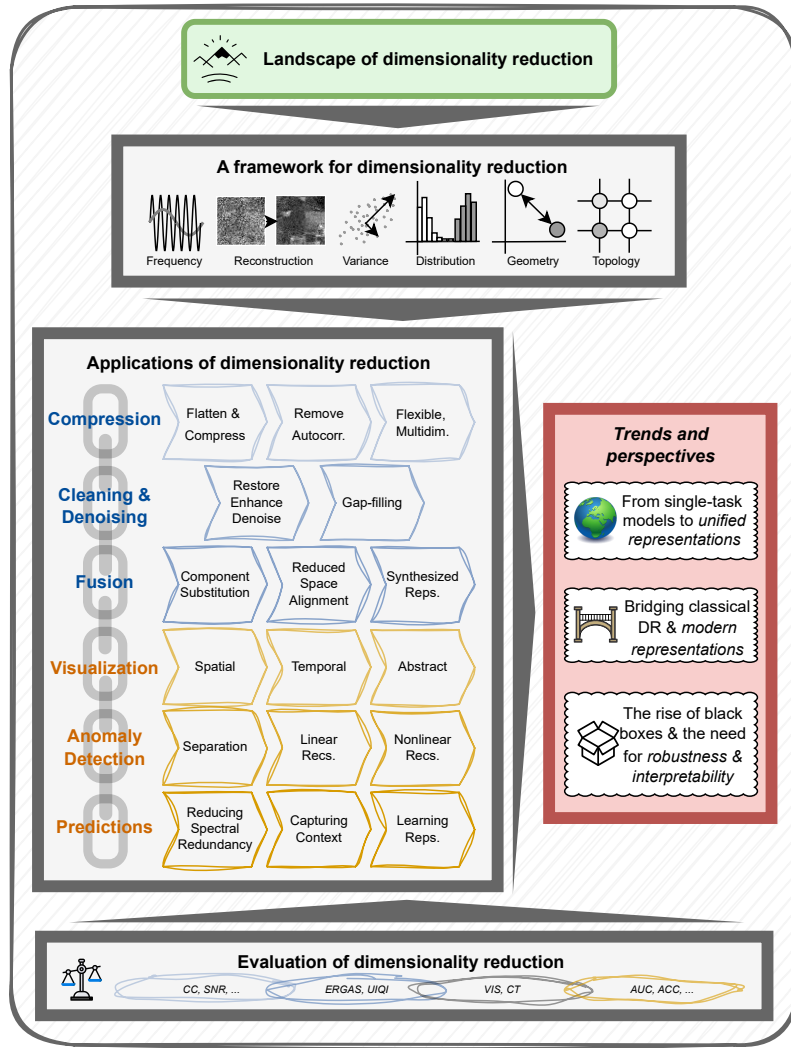


Figure 3: **A graphical abstract for DR in RS.** We provide *a framework for DR* and use it to characterize standard DR methods in RS within the complex landscape of DR (see Sec. 2). Once organized, these methods are tracked across the RS data value chain, as we traverse the *applications of DR* in RS (see Sec. 3). Then, we present application-specific *evaluation of DR* (see Sec. 4). Finally, the trends of DR in RS are synthesized, yielding three key perspectives for the future of DR in the foundation model era (see *trends and perspectives*, Sec. 5).

2. A framework for dimensionality reduction

The field of Dimensionality Reduction (DR) is expansive and populated with a zoo of algorithms ranging from linear multivariate analysis and manifold learning to deep learning. Selecting an appropriate DR technique for a given RS task can be challenging. Our novel framework, illustrated in Fig. 4, structures the field of DR, thus providing a practical guide for researchers. We characterize DR methods into families based on three axes: the input dataset (Sec. 2.1), the mapping (Sec. 2.2), and the properties preserved (Sec. 2.3).

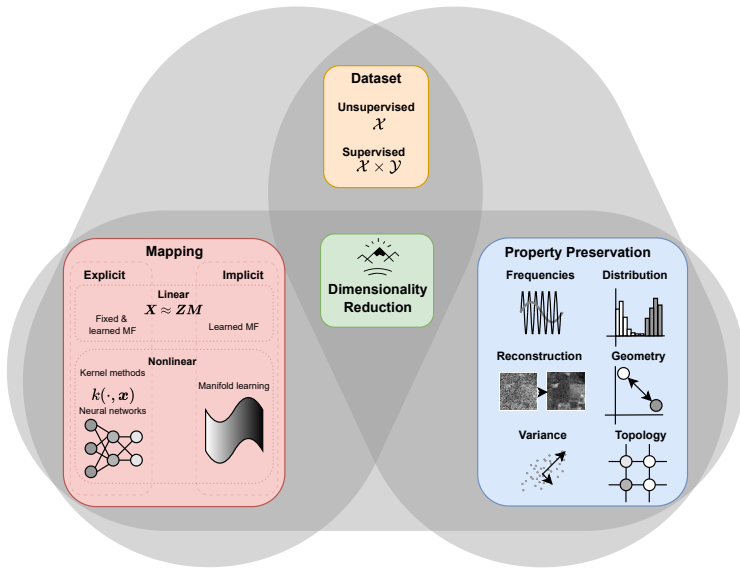


Figure 4: **A framework of DR.** DR characteristics are separated into the three pillars: mapping, dataset, and property preservation. The DR mapping can be either explicit or implicit and either linear or nonlinear. We separate classes of DR mappings by their mapping mechanism: fixed or learned matrix factorization (MF), kernel methods, neural networks, and manifold learning. Different DR methods are used for different tasks based on the input dataset. Unsupervised DR methods just input a dataset $\mathcal{D} \subset \mathcal{X}$, whereas supervised methods take a dataset of pairs $\mathcal{D} \subset \mathcal{X} \times \mathcal{Y}$ as inputs. The property preservation for DR algorithms includes data frequencies, reconstructions, variance, distributions, geometry, and topology.

Historically popular DR methods in RS are placed in our framework in Fig. 5. Using this framework, a practitioner can navigate the DR landscape to identify a family of algorithms best suited for their goal.

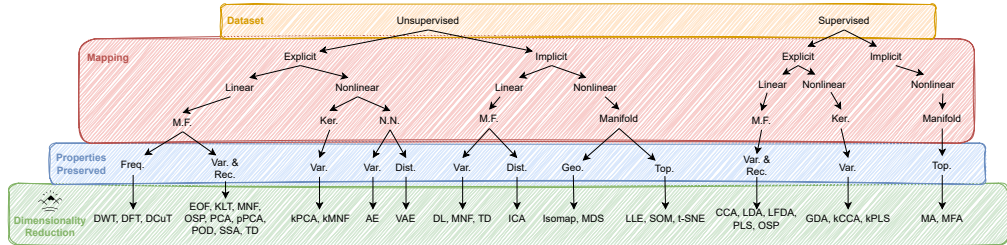


Figure 5: Common DR in RS characterized by their dataset, mapping, and properties preserved. We use the following abbreviations for mapping mechanisms: M.F. for matrix factorizations, Ker. for kernel methods, N.N. for neural network, and Manifold for manifold learning. For properties preserved we abbreviate frequencies and signal structure as Freq., variance and reconstruction as Var. & Rec., distribution as Dist., geometry as Geom. and topology as Top.

2.1. Dataset

The *dataset* \mathcal{D} is the input data to DR and contains N samples in the high, P -dimensional, ambient space. We characterize DR methods as supervised or unsupervised based on the structure of the input dataset. For supervised DR methods, our input dataset consists of a set of N paired samples $\mathcal{D} = \{(\mathbf{x}_1, \mathbf{y}_1), \dots, (\mathbf{x}_N, \mathbf{y}_N)\} \subset \mathcal{X} \times \mathcal{Y}$, where \mathcal{X} is the ambient space and \mathcal{Y} contains auxiliary information (e.g., class labels) that guide the reduction process. In contrast, unsupervised methods do not rely on such labels, and the input dataset is only $\mathcal{D} = \{\mathbf{x}_1, \dots, \mathbf{x}_N\} \subset \mathcal{X}$. Notably, self-supervised DR techniques do not rely on external labels but instead create pseudo-labels from the inherent data structure, and thus are unsupervised methods.

2.2. Mapping

Regardless whether or not a DR method is supervised, the input RS data is high-dimensional, redundant, corrupted by noise, and challenging to interpret. DR reduces the feature dimension of an input dataset from a high, P -dimensional ambient space to a low, K -dimensional reduced space. In the reduced space, the extracted features capture the essential information of the data in fewer dimensions, often eliminating redundancy and noise while enhancing interpretability. This transformation is done by the DR mapping.

DR mappings can be either explicit or implicit. *Explicit DR* mappings, denoted ϕ , transform the ambient features into reduced features, whereas *implicit DR* outputs the reduced data without defining the mapping ϕ . Thus, explicit DR can be applied to new data using ϕ , whereas implicit DR cannot. In explicit DR, an (often approximate) inverse DR mapping (denoted $\psi(\cdot) \approx \phi^{-1}(\cdot)$) can be either learned or directly computed from ϕ . The inverse DR mapping allows us to reconstruct the data from its reduced representation enabling tasks in RS, like denoising.

Beyond explicit and implicit mappings, DR mappings are separated into linear and nonlinear. *Linear DR* has lower computational complexity, higher interpretability, and often a closed-form solution. In contrast, *nonlinear DR* captures more complex nonlinear relationships between data. For explicit DR, the linear vs nonlinear dichotomy refers to the structure of ϕ . Whereas for implicit DR, we distinguish between linear and nonlinear methods based on the ability of the technique to preserve nonlinear structures in the data. Overall, while nonlinear methods showcase impressive advantages [95], linear techniques remain valuable in various practical scenarios.

We now characterize different linear and nonlinear DR methods by their mapping mechanism. The primary mapping mechanism for linear DR methods is *matrix factorization*, meaning that they factor the high-dimensional data matrix $\mathbf{X} \in \mathbb{R}^{N \times P}$ (samples \times ambient features) into a mixing matrix (sometimes called dictionary) $\mathbf{M} \in \mathbb{R}^{K \times P}$ and the matrix storing the reduced representations $\mathbf{Z} \in \mathbb{R}^{N \times K}$ as $\mathbf{X} \approx \mathbf{ZM}$. Matrix factorizations are divided into fixed factorizations (e.g., predefined \mathbf{M}) and those with learned factorizations (e.g., learned \mathbf{M}). Respective examples of fixed factorizations and learned factorizations are the Discrete Wavelet Transform (DWT) [18] and Principal Component Analysis (PCA) [72]. Fixed matrix factorization methods are often explicit, whereas learned matrix factorizations are divided into implicit methods, like Dictionary Learning (DL) [93], and explicit methods, like DWT and PCA.

The other family of mapping mechanisms, nonlinear DR, is divided into three mapping mechanisms: kernels, neural networks, and manifold learning. *Kernel methods* are a large family of non-linear explicit DR methods that use a kernel mapping mechanism [24]. These methods use the kernel trick to generalize classical linear DR methods to nonlinear methods, like kernel PCA (kPCA) [153], by applying them in a high-dimensional (potentially infinite) feature space \mathcal{H} . The foundation of kernel methods is the kernel trick, which circumvents the need to specifically compute a mapping φ into

\mathcal{H} while allowing us to compute properties in that space directly. It does this through the kernel function k , enabling the computation of similarities in the feature space as

$$k(\mathbf{x}_n, \mathbf{x}_m) = \langle \varphi(\mathbf{x}_n), \varphi(\mathbf{x}_m) \rangle_{\mathcal{H}}. \quad (1)$$

The most popular kernel function, the RBF Kernel, is “universal,” i.e., it can approximate any function uniformly [126].

A second family of explicit nonlinear DR methods uses a *neural network* mapping mechanism to parameterize DR mappings. For example, Autoencoders (AEs) [12] are a flexible DR method that learns a DR mapping (encoder) and its approximate inverse (decoder) by minimizing a loss function. Design choices for the neural network methods include the number of layers and hidden units, the type of nonlinearity, and the properties preserved in the loss function. Recently, deep neural network methods have gained popularity as they enable training models with millions of parameters and the assimilation of vast amounts of data. Neural network methods offer high flexibility, albeit at the cost of reduced interpretability.

Both kernel methods and neural networks are explicit DR mappings; most implicit nonlinear DR uses a *manifold learning* mapping mechanism. These methods optimize directly for the reduced data representation, often aiming to mirror the ambient data manifold structure in the reduced space through preservation of geometric or topological properties. One of the most popular manifold learning DR methods for data visualization is t-distributed Stochastic Neighborhood Embedding (t-SNE) [119].

2.3. Property preservation

The distinction between different property preservation goals is the core utility of our DR framework. Most families, other than frequency and signal-structure preserving DR, preserve properties from the ambient space in the reduced space by defining DR methods as solutions to optimization problems. The inputs for the objective function can be the ambient data, reduced data, DR mapping, and/or its approximate inverse. Then, the objective function returns a value representing how well the property of interest is preserved.

Frequency and signal-structure preserving. A small family of DR methods designs a pre-defined DR mapping to *preserve frequency and other signal structures* in the reduced space. These transforms are a simple and computationally efficient, task-agnostic family of DR methods. They prescribe a

linear DR mapping $\Phi \in \mathbb{R}^{K \times N}$ and approximate inverse $\Psi \in \mathbb{R}^{N \times K}$ in

$$\mathbf{z} = \Phi \mathbf{x}, \quad \mathbf{x} \approx \Psi \mathbf{z}, \quad \Phi \text{ fixed.} \quad (2)$$

These mappings are often aligned to the desired signal structure through a basis of functions. The DWT is a classic example of these methods as it uses a mother wavelet to build Φ , and it preserves both signal location and scale in the reduced space.

Variance preserving. Variance-preserving methods, like the unsupervised PCA and the supervised Partial Least Squares (PLS) [57], use a trace-ratio objective in Eq. 3 where \mathbf{A} encodes the signal we want to preserve and \mathbf{B} encodes the noise or irrelevant directions in the data.

$$\max_{\mathbf{M}} \frac{\text{tr}(\mathbf{M}\mathbf{A}\mathbf{M}^{\top})}{\text{tr}(\mathbf{M}\mathbf{B}\mathbf{M}^{\top})} \quad (3)$$

Classical variance-preserving methods are explicit and linear and thus incapable of capturing nonlinear structures in the reduced space. Kernel methods generalize most of these classical DR methods from trace-ratio problems to nonlinear, explicit, variance-preserving methods, like kPCA [153] and kernel PLS (kPLS) [57].

Reconstruction preserving. Some variance-preserving methods, like PCA can also be viewed as reconstruction-preserving methods because, under certain conditions, reconstruction minimization is equivalent to trace maximization. Specifically,

$$\underset{\mathbf{M}\mathbf{M}^{\top}=\mathbf{I}}{\text{argmin}} \|\mathbf{X} - \mathbf{X}\mathbf{M}^{\top}\mathbf{M}\|_F = \underset{\mathbf{M}\mathbf{M}^{\top}=\mathbf{I}}{\text{argmax}} \text{tr}(\mathbf{M}\mathbf{X}^{\top}\mathbf{X}\mathbf{M}^{\top}).$$

However, not all reconstruction preserving methods are variance-preserving. These methods include dictionary learning, tensor factorization, and autoencoders.

Thus far, we have touched on DR methods with fixed constraints (e.g., orthogonality) that lack the flexibility necessary for some RS tasks. *Dictionary Learning* (DL) [93] offers an alternative to these variants through learned matrix factorization (e.g., implicit, linear DR) that aims to preserve data reconstructions while satisfying constraints \mathcal{C} on \mathbf{Z} , and/or the dictionary, \mathbf{M} (see Eq. 4).

$$\min_{\mathbf{M}, \mathbf{Z}} \|\mathbf{X} - \mathbf{M}\mathbf{Z}\| \quad \text{s.t. } \mathbf{M}, \mathbf{Z} \in \mathcal{C}. \quad (4)$$

For instance, when modeling a known physical process, one may want to enforce this constraint because negative entries would contradict the physical understanding of the process (e.g., temperatures in Kelvin). Non-negative Matrix Factorization (NMF) [190] adds these hard constraints to the optimization problem by enforcing positive entries in \mathbf{M} and \mathbf{Z} .

Although diverse and useful, these matrix-based approaches, like PCA, kPCA, and DL, are misaligned with the structure of most RS data. Most RS data arrives in 3-dimensional tensors with spatial (latitude and longitude) and spectral dimensions. *Tensor Decomposition* (TD) methods [186] generalize matrix-based DR methods to tensors by jointly reducing multiple dimensions of RS data within a single decomposition framework. The most common TD method is the Tucker decomposition, which generalizes the singular value decomposition (SVD) used in matrix DR methods such as PCA and DL to tensor inputs. Thus, TD methods can be both variance and reconstruction preserving.

More modern, flexible, and nonlinear DR actually learns DR mappings (encoder ϕ and decoder ψ) parameterized by neural networks by minimizing a loss function \mathcal{L}

$$\min_{\phi, \psi} \mathcal{L}(\mathbf{X}, \phi, \psi). \quad (5)$$

using gradient descent variants [148]. The typical example of these methods are AEs. Although AEs were initially designed to minimize only reconstruction error, they can optimize any sufficiently smooth objective function \mathcal{L} and thus incorporate various regularizers enforcing properties of interest (e.g., physical, causal, probabilistic, geometric, and topological) [12]. However, this flexibility of AEs comes at a cost. AEs often lack interpretability, theoretical guarantees, require many samples to properly fit the data, and are computationally expensive to train.

Distribution preserving. Distribution-preserving methods partially remedy the lack of theoretical guarantees of AEs by imposing a statistical model on the reduced data distribution, resulting in robust models that are statistically consistent across observations. These methods are exemplified by the Variational AE (VAE) [88], which learns a generative model of the data. Specifically, the VAE models a reduced (a.k.a. latent) space prior $p(\mathbf{z})$ with an encoded probability $q_\phi(\mathbf{z}|\mathbf{x})$ and produces reconstruction probabilities $p_\psi(\mathbf{x}|\mathbf{z})$. Then, VAEs optimize the data representations by maximizing the Evidence

Lower Bound (ELBO)

$$\text{ELBO}(\phi, \psi, \mathbf{x}) = \mathbb{E}[\log p_\psi(\mathbf{x}|\mathbf{z})] - D_{\text{KL}}(q_\phi(\mathbf{z}|\mathbf{x}) || p(\mathbf{z})).$$

The first term ensures reconstruction accuracy, while the Kullback–Leibler (KL) term enforces regularity of the reduced space distribution.

Geometry preserving. Remote sensing data is often governed by a small number of continuous parameters. Under smooth forward models, moderate noise, sufficient sampling density, and few regime changes, this implies that the data concentrate near low-dimensional manifolds embedded in the ambient space. These manifolds are locally Euclidean and thus can be partially captured locally by linear DR methods. However, linear methods miss the global structure of the nonlinear data manifold. Although some methods discussed so far are nonlinear, they neither directly preserve the manifold geometry nor its topology. Implicit, nonlinear DR, known as manifold learning, assumes that high-dimensional data lie on a low-dimensional manifold and aims to preserve either the global geometry or the local topology in the reduced space.

Early attempts, like Multidimensional Scaling (MDS) [151], *preserve global geometry* through matching distances between ambient and reduced spaces, e.g.,

$$\min_{\{\mathbf{z}_n\}_{n=1}^N} \sum_{n>m}^N (d_{n,m} - \|\mathbf{z}_n - \mathbf{z}_m\|_2)^2. \quad (6)$$

Standard MDS fails to capture local structures because the chosen ambient space distance between points n and m (denoted $d_{n,m}$) is often not the true distance measure on the data manifold. Isomap [9] improves estimation of $d_{n,m}$ by using geodesic distances, thus better capturing the true data manifold structure.

Topology preserving. The community quickly moved past global geometry-preserving DR to local topology-preserving DR in an aim to preserve neighborhood structures in the reduced space ¹. One of the first methods in this paradigm, Locally Linear Embedding (LLE) [152], uses nearest-neighbor

¹While early prototype-based methods like Self-Organizing Mappings(SOM) [92] attempted to preserve topology by fitting a grid to data, the modern paradigm is data-driven, building a graph from the ambient dataset.

graphs to preserve local structures. Although LLE is a theoretically sound DR method, it requires a smooth data manifold with well-sampled data and consistency between locally linear patches.

Trading the geometric faithfulness of LLE for visual separability, t-SNE is a widely used local topology-preserving DR method. t-SNE models both the ambient and reduced data using similarity graphs based on the RBF kernel. Then, it uses a probabilistic approach to align the edge distribution of the reduced graph Q to the ambient graph P . Using $p_{n,m}$ as the edge weight between node n and m in P and $q_{n,m}$ as the modeled edge weight in Q , t-SNE minimizes the KL divergence between P and Q :

$$D_{\text{KL}}(P||Q) = \sum_{n>m} p_{n,m} \log \left(\frac{p_{n,m}}{q_{n,m}} \right)$$

via gradient descent. Since t-SNE is an iterative method, careful treatment of the initial conditions leads to better-reduced spaces [91]. Although t-SNE preserves local neighborhoods, resulting in clustered low-dimensional embeddings, it suffers from high computational cost, sensitivity to perplexity, and a non-convex objective.

2.4. Synopsis

Our characterization of DR methods provides a clear framework for navigating the landscape of DR techniques. It is built on three pillars: the input dataset, the mapping, and the properties preserved. While the dataset and mapping criteria create a mutually exclusive and collectively exhaustive classification, property preservation does not, as a single method can serve multiple objectives.

This framework for DR is not merely a catalog; it is a tool designed to guide practitioners in the selection of appropriate algorithms for their applications. The complete taxonomy of common DR methods in RS using our framework is visualized in Fig. 5 and serves as a practical decision-making guide for any RS practitioner. For a quick reference, all common DR methods in RS are listed in the glossary; see Tab. A.5. Now, armed with a structured understanding of common DR in RS, we are ready to analyze how these methods improve tasks in the RS data value chain. By applying this framework to the literature, we can extract underlying patterns, revealing why certain families of DR methods are consistently used for specific tasks in the RS data value chain.

3. Applications of dimensionality reduction

Having established our DR framework, we use it now as a guide to follow an RS dataset through the data value chain. In doing so, we will move *beyond HS data*, given the varied needs for DR across data types (see Fig. 1). This journey begins with preprocessing tasks: compression, cleaning, and fusion of raw remote sensing data. Then we proceed to the essential analysis stage, where DR is used for visualization, anomaly detection, and ultimately for empowering predictive models to generate improved scientific insight. The content of this section is summarized in Tab. 1.

3.1. Pre-processing

The goal of pre-processing is to prepare raw RS data by isolating the underlying signal from noise and atmospheric effects. Raw RS data is often high-volume and high-complexity, thus necessitating compression for easy transport and storage. These data also require additional cleaning and denoising steps to ensure that sensor artifacts, noise, and misregistration do not dominate the signal. Once the signal is isolated, a wide variety of RS data modalities and resolutions from different sensors (see Fig. 1) are often fused to accomplish a specific task. DR techniques themselves are the primary engines of these pre-processing tasks, empowering the core tasks of compression (3.1.1), data cleaning (3.1.2), and fusion (3.1.3).

3.1.1. Compression

Data compression reduces the dimensionality of remote sensing data while extracting important information, improving downstream tasks, like parameter retrieval, unmixing, and classification [56, 54]. Specifically, it addresses challenges involving limited transmission channel bandwidth, transmission time, and storage space by removing redundant information from data on-board platforms (e.g., satellites, drones) and on the ground.

Data compression is divided into two tasks: lossless and lossy compression. Lossless compression reduces data volume while preserving perfect reconstruction, whereas lossy compression allows some information loss. *We only consider DR for lossy compression* because DR reconstructions are generally imperfect. Algorithms for lossy compression consist of an encoder, a bitstream translation, and a decoder. A DR method for RS compression is almost always unsupervised using an explicit mapping to provide an encoder and decoder via ϕ and ψ .

Table 1: **A summary of how, within our framework, DR addresses each challenge in the RS data value chain.** First, we decompose each RS challenge into stages. Then we use our framework for DR in RS to identify the common DR characteristics for each stage, namely the dataset, mapping, and properties preserved. Next, we list common DR methods at each stage, and finally list references to specific applications where DR is used in this context. We abbreviate following mapping mechanisms: matrix factorization (MF), kernel (Ker), neural network (NN), and manifold learning (Man).

Challenge	Stage	Dataset	Mapping	Properties preserved	DR Methods	References
Compression	Flatten & Compress	Unsupervised	Linear, MF	Frequency, variance, reconstruction, distribution	DFT, DWT, ICA, NMF, PCA	[15, 82, 163, 185, 154]
	Removing autocorrelation	Unsupervised	Explicit, linear, MF	Frequency, variance	DWT, PCA	[135, 45, 136]
	Flexible, multidimensional compression	Unsupervised	Explicit, linear, nonlinear, MF, NN	Reconstruction	AE, TD	[86, 55, 197, 133]
Data Cleaning	Image restoration, enhancement and denoising	Unsupervised	Explicit, implicit, linear, nonlinear, MF, NN	Frequency, variance, reconstruction	DWT, MNF, PCA, AE	[33, 47, 114, 140, 192]
	Gap Filling	Unsupervised	Explicit, implicit, linear, nonlinear, MF, NN	Frequencies, variance, reconstruction	AE, DCT, DL, PCA	[158, 201, 102, 42, 43, 139, 162, 83, 184]
Fusion	Component Substitution	Unsupervised	Explicit, linear, MF	Frequency, variance	DWT, PCA	[32, 115, 205, 155, 204]
	Alignment of a Shared Reduced Space	Unsupervised, supervised	Explicit, implicit, linear, nonlinear, MF, Ker, Man	Variance, reconstruction, topology	CCA, kPCA, LLE, PCA, MA	[109, 199, 175, 103, 40, 58, 121]
	Synthesized Representations with Deep Learning	Unsupervised, supervised	Explicit, nonlinear, NN	Reconstruction	AE	[75, 105, 74, 156, 64]
Visualization	Spatial	Unsupervised	Explicit, implicit, linear, nonlinear, MF, Man	Variance, reconstruction, topology	PCA, SOM, LLE	[26, 62, 170, 127, 8]
	Temporal	Unsupervised	Explicit, linear, nonlinear, MF, NN	Variance, reconstruction, distribution	PCA, VAE	[71, 13, 21, 149, 77]
	Abstract	Unsupervised	Implicit, nonlinear, Man	Geometry, topology	Isomap, LLE, t-SNE	[165, 209, 150]
Anomaly Detection	Separation	Supervised	Implicit, linear, nonlinear, MF, Man	Reconstruction, geometry	DL, MDS	[169, 131, 44, 117, 166, 171, 35]
	Linear Reconstruction	Unsupervised	Explicit, linear, MF	Frequency, variance	DWT, PCA	[79, 45, 120, 47, 208, 51]
	Nonlinear Reconstruction	Unsupervised	Explicit, implicit, nonlinear, NN, Ker	Variance, reconstruction	AE, kPCA, MDS	[63, 207, 160, 198, 111, 195, 50, 76, 196, 187]
Predictions	Reducing Spectral Redundancy	Unsupervised, supervised	Explicit, implicit, linear, nonlinear, MF, Man	Frequency, variance, reconstruction, geometry, topology	DCuT, DWT, Isomap, LFDA, LLE, PCA	[69, 136, 176, 20, 55, 138, 100, 101, 112, 8]
	Capturing Context	Unsupervised, supervised	Explicit, implicit, linear, nonlinear, MF, Ker, Man	Frequency, variance, reconstruction, topology	DFT, kPCA, MA, TD	[108, 86, 40, 103, 58, 175, 146, 17, 173]
	Learning Representations	Unsupervised, supervised	Explicit, nonlinear, NN	Reconstruction	AE	[113, 1, 156, 85, 118, 7, 90, 110, 38, 123]

Flatten & compress. RS data naturally contains spatial, spectral, and temporal dimensions. Initially, dimensions were compressed individually, or combinations of dimensions were flattened, then compressed. Originally, linear matrix factorization DR methods that preserve frequency, variance, reconstruction, and/ or distributions (e.g., DFT, PCA, and ICA) were tested for compression of RS data [15, 82]. These methods were surpassed by the foundation for RS data compression, JPEG2000 [163]. This method breaks the image into tiles and utilizes the DWT to compress the spectral dimension. Although other, more flexible implicit DR methods, like NMF, have been tested for compression [185], DWT-based compression remained the baseline DR method, proving effective for compressing even ultraspectral sounder data [154]. Overall, linear DR methods, with pre-defined mappings that preserve frequency and signal structure, have proven to be solid baseline compression methods.

Removing autocorrelation. Autocorrelation in the spectral bands of Multi-spectral (MS) and Hyperspectral (HS) data leads to spectral redundancy that is ineffectively compressed by standard JPEG compression. Pre-processing with the linear, explicit, frequency, and reconstruction-preserving DR like 3D DWT [135] and PCA variants [45, 136] decorrelates these bands, thus reducing spectral redundancy and improving the effectiveness of subsequent DWT compression.

Flexible, multidimensional compression. Although promising advances have been made, these methods either compress each dimension individually or flatten dimensions of spatio-temporal data cubes before applying compression, thereby missing the structure of RS datasets. An initial remedy for this issue is video compression as it is a promising method for faithful compression of both spatial and temporal dimensions [133]. A more general solution is TD methods because they generalize traditional linear matrix factorization methods to handle the data cube in its natural form, thereby preserving its inherent structure. For example, the Tucker decomposition improves upon DWT-based compression [86]. In general, TD methods are highlighted as a promising research direction for HS compression DR [55].

Due to increases in computation power and, consequently, the rising popularity of deep learning, DR methods for compression no longer need to be rigid matrix factorizations. Consequently, learnable neural network DR shows promise for modern RS data compression. For example, AEs improve

data compression flexibility by learning optimal nonlinear transforms directly from data rather than using a fixed DWT or TD basis [197].

3.1.2. Data cleaning

Data cleaning addresses problems involving data quality during the pre-processing phase. For example, cloud cover affects the usability of optical satellite imagery [137] and atmospheric interference introduces noise and reduces land cover classification rates [179]. Data cleaning addresses these problems by either separating signal from noise via image restoration, enhancement, and denoising, or by generating new information to fill in missing data. In general, these tasks are performed in spatial, temporal, and/or spectral dimensions and include cloud, shadow, and haze removal, as well as sensor error correction, such as image de-striping [159, 25]. DR for data cleaning leverages reconstructions from the reduced space to generate uncorrupted images.

Image restoration, enhancement and denoising. Denoising can be done individually in each dimension of the HS image or simultaneously in multiple dimensions through unsupervised DR. Linear, frequency, variance, and reconstruction preserving methods (e.g., DWT, PCA, and MNF) work by concentrating the signal structure into a few reduced components and discarding the “noise” in the remaining components. The DWT and PCA are combined for denoising HS data [33]. PCA has also been adapted for LiDAR denoising [47] and compared to MNF for denoising HS data [114].

As with compression, denoising DR has moved from these linear baselines to more flexible, explicit and nonlinear deep learning methods. For example, the untied denoising AE is designed for denoising HS data and outperforms state-of-the-art methods in high-noise regimes for spectral unmixing [140]. Finally, a contrastive learning approach that pairs clean, noisy, and denoised images in the representation space has outperformed other deep learning approaches in denoising 3-channel images [192].

Gap-filling. In gap-filling, there is no signal to separate. The goal is to generate data by learning from the spatial, spectral, and temporal context. We focus on two case studies for gap-filling, namely cloud/shadow replacement and temporal gap filling.

Cloud/shadow replacement is one of the most common spatial gap-filling tasks. DR methods for cloud replacement are generally supervised because

they use cloudless reference images from different spatial locations or the same spatial location at other times, and/or other data modalities [158]. In general, DR methods for this task combine reduced representations or DR mappings of cloudy and reference images to replace missing data. Supervised variants of DL-based methods align dictionaries to replace clouds in HS and MS datasets (e.g., Hyperion, OLI, Landsat, and MODIS) [102, 201].

The frontier of cloud replacement employs deep learning methods, such as AEs, that excel at learning complex contextual relationships. For example, such methods effectively replace clouds in SST measurements [43] and MS data [42]. A review of gap-filling using convolutional neural network architectures highlights the utility of these AEs architectures [139].

In contrast with cloud and shadow replacement, DR methods for time-series gap-filling in RS have yet to adopt deep learning and continue to use linear methods that preserve variance and frequency. For example, PCA is used for reconstructing surface chlorophyll, total suspended matter, and sea surface temperature data [162] along with MODIS leaf area index products [83]. Furthermore, frequency-preserving DR, like the Discrete Cosine Transform (DCT), has been incorporated into a specialized algorithm to replace missing soil moisture data [184].

3.1.3. Fusion

The challenge of harmonizing different RS data modalities and resolutions for joint analysis is called fusion. Algorithms for fusion must be computationally efficient, preserve high resolution, and reduce color distortion. Fusion is carried out at different levels: pixel, feature, or decision level [59]. We focus on pixel and feature-level fusion where DR is most beneficial. Fusion is divided into *homogeneous fusion* and *heterogeneous fusion*. The former uses only single-modal data and can be applied to any gridded data by matching image locations and applying pixel-level operations. The latter is more modern and flexible because it integrates a broader range of sources. DR has evolved for data fusion through 3 eras, generally moving from homogeneous tasks to more general, heterogeneous tasks. These eras are component substitution, alignment of a shared reduced space, and learning synthesized representations with deep learning. Throughout these eras, the best models are often supervised and have moved from explicit, linear DR that preserves variance and frequency, to implicit, topology-preserving DR, and finally to flexible deep learning DR with neural network mapping mechanisms.

Component substitution. The earliest strategies, like Component Substitution (CS), are explicit, linear DR that were primarily developed for homogeneous fusion, i.e., pansharpening. CS is simple, it runs PCA on the low-resolution image, then substitutes the leading principal components with the high-resolution pan image, and finally maps the new reduced representation back to the ambient space [32]. In applications, CS offers benefits in low color distortion but suffers from spectral distortion in MS and HS data. Various pre-defined matrix factorization DR, such as wavelet, contourlet, or support value transforms, are run before CS to address the persistent challenge of spectral distortion in the fused images [115, 205, 155, 204]

Alignment of a shared reduced space. Limitations of CS, such as its difficulty in handling spectrally diverse datasets, motivated the next step in DR for fusion, paving the way for tools for both homogeneous and heterogeneous tasks. These tools exchange the PCA-reduced space for a more general, nonlinear shared reduced space.

In homogeneous fusion, supervised topology-preserving manifold learning techniques like Locally Linear Embedding (LLE) and semi-supervised Manifold Alignment (MA) achieve this by preserving local structure. Specifically, LLE reduces bias by capturing structural differences among image patches [109, 199]. Semi-supervised MA builds upon LLE and has been used to align multi-temporal, multi-angle, and multi-source RS data to improve classification rates [175].

Early heterogeneous fusion uses PCA as a shared feature extractor for graph-based fusion of optical-thermal-hyperspectral data [103] and HS-LiDAR [40]. kPCA improves linear, PCA-based fusion by finding a nonlinear shared space for HS-LiDAR fusion [58] while supervised methods like CCA have been applied to fuse MS and LiDAR data for improved forest structure characterization [121].

Synthesized representations with deep learning. Nowadays, deep learning drives the data fusion paradigm through learning optimal end-to-end synthesis of remote sensing datasets. In homogenous fusion, sparse deep AEs [75] achieve high spatial resolution while mitigating spectral distortion. This was further refined by introducing independent encoders for each source [105]. This technique has been extended with adaptive PCA and multi-scale DNNs [74]. In heterogeneous fusion, deep AEs have been used to integrate LiDAR, SAR, and satellite optical data to map above-ground forest biomass [156].

Beyond the autoencoder, a modern deep learning method called contrastive learning has been applied to fusion tasks. When co-registered images are available, contrastive learning can encourage representations from different modalities to be similar, thereby implicitly performing fusion. This approach has shown superior performance when pretraining on Sentinel-1 and Sentinel-2 data for land cover classification [64].

3.2. Analysis

The analysis stages of the RS data value chain begin to extract real scientific meaning from the datasets. First, data visualizations explore datasets, constructing maps and identifying patterns that can be used to build hypotheses (Sec. 3.2.1). Then, anomaly detection identifies unexpected patterns and outliers, such as extreme events or crop failures (Sec. 3.2.2). Finally, RS data is quantified in predictions, the ultimate goal of the RS data value chain, turning data understanding into actionable forecasts and scientific conclusions (Sec. 3.2.3). For each of these pursuits, DR is a critical tool for improving these tasks by extracting essential low-dimensional representations from complex high-dimensional data.

3.2.1. Visualization

As a picture is worth a thousand words (or, in the era of big data, even a million), visualization aims to summarize data, reveal patterns and structures, and thus extract information in a way that is easy for the human eye to interpret. We categorize DR algorithms for visualization based on the axes they reduce and the information they aim to preserve: creating interpretable maps, identifying dynamic patterns, and uncovering hidden spatial structures.

Spatial visualizations. In DR, spatial visualizations reduce spectral features to 1 to 3 bands and display them as a map, which can evolve to track changes. This enables analysis of spatial patterns, such as vegetation changes, urbanization, or cloud cover. The most straightforward approach to reducing the spectral domain is PCA, which helps generate informative color maps that outperform traditional False Color Composites (FCCs), particularly as satellite sensors become more advanced [26].

Spatial visualizations quickly moved beyond explicit linear DR to implicit DR that preserves topology. At first, SOMs were a common approach for visualizing HS data and have been extended to output to a three-dimensional

cube, mapping the data into an RGB subspace for enhanced visualization [62, 170]. However, both SOM and PCA fail to coherently preserve both local and global structures and thus struggle with larger scenes.

Advancements in manifold learning for RS data visualization have overcome this challenge, ensuring more coherent visual representations by capturing local and global structures in the data. For example, Najim et al. demonstrate that nonlinear LLE improves cluster separation and thus outputs a more meaningful spatial visualization. Due to computational constraints, an HSI must be divided into smaller tiles, after which FCCs can be computed for each tile [127]. Finally, these FCCs must be aligned to produce one coherent FCC. Groundbreaking work by Bachmann et al. uses Isomap to produce FCCs for each tile, then uses LLE to align these tiles, thus creating coherent, structure-preserving maps of large areas [8].

Temporal visualization. Many applications (e.g., climate and atmospheric sciences) focus on temporal changes. DR to enable the identification of these changes often reduces the spatial and/ or spectral dimension of RS data. For example, PCA variants are standard techniques in climate science for extracting modes of climate variability—time series representing complex spatiotemporal phenomena—and identifying teleconnections — statistical dependencies between modes [71, 13]. Although ubiquitous in fields such as climate science, PCA cannot capture the nonlinear dynamics of the Earth system.

More recent approaches have extended PCA to application-specific methods that capture more subtle, complex climate variability. Variants such as the non-linear ROCK-PCA [21] and rotated Varimax PCA [149] have been used to decompose spatiotemporal datasets of different climate variables, extracting seasonality and modes of variability. Enabling higher flexibility and capturing nonlinearities, deep learning techniques have also been applied to improve climate indices. For example, [77] demonstrated that VAEs explain more variability in the North Atlantic Oscillation (NAO) than traditional PCA-based approaches.

Visualization in an abstract space. In this setting, DR reduces one or a combination of RS data dimension samples to a 2-3 dimensional space to form hypotheses about the data. We compare DR methods for visualization in an abstract space in Fig. 6. Although DR for visualization began with unsupervised, explicit, linear DR that preserves variance, it quickly shifted to

nonlinear methods that preserve the topology of the data manifold. For example, Song et al. enhanced t-SNE by integrating it with a Gaussian Mixture Model, improving its ability to represent HS data [165].

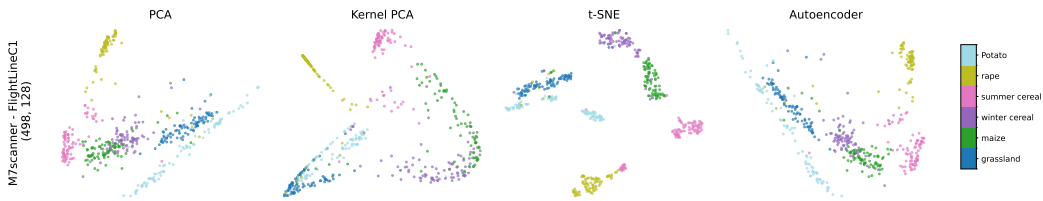


Figure 6: **Two-dimensional embeddings of spectral data generated using various dimensionality reduction techniques.** The data originates from the HyperLabelme dataset [122], specifically from the FlightLineC1 site and the M7scanner sensor. The dimensionality reduction algorithms were trained on 498 samples, each with a spectral dimensionality of 128.

Now, in the age of general and black-box abstract feature spaces from neural network parameterized deep learning models, DR can be used to interpret these features. For example, applying t-SNE to the feature spaces learned by deep learning models improves interpretability, enabling the development of hypotheses for how the model distinguishes between classes [209, 150].

3.2.2. Anomaly detection

Anomaly detection involves identifying samples that differ substantially from the majority of data within a dataset. We classify anomalies into point, collective, or contextual. Point anomalies are single instances deviating from the rest of the data, collective anomalies consist of multiple related instances that are anomalous when combined, and contextual anomalies depend on the surrounding context for their abnormality [30]. Flach et al. demonstrated that effective feature extraction via DR can be more crucial for detecting spatiotemporal extremes than the choice of detection algorithm [52]. DR techniques can improve anomaly detection across spectral, spatial, and temporal dimensions because they may only become apparent in the reduced space or because of poor reconstructions. DR for anomaly detection in RS follows two distinct models: the separation model and the reconstruction model.

The separation model. The separation model explicitly separates the data into background and anomaly components and is generally used for spectral anomalies. In this model, reconstruction-preserving DR methods with implicit mappings impose mathematical constraints to directly decompose the data as a sum of background and anomaly. For example, low-rank DL models decompose HS data into a structured low-rank component and a sparse anomaly component. Spatial constraints refine this process by enforcing local consistency, ensuring that anomalies align with expected spatial patterns rather than appearing as isolated noise [169]. DL adapts basis functions to HS data, improving feature separation compared to PCA [131]. Discriminative metric learning optimizes DL to maximize spectral contrast, enhancing robustness [44]. Sparse representation models extend this concept by applying DL to anomaly detection in HS data [117].

Nonlinear DR is also used as part of the separation model. For example, geometry-preserving manifold learning, like MDS, have successfully quantified earthquake damage by comparing pre-event optical images with post-event SAR images [171]. Other nonlinear DR directly build of DL, resulting in hybrid models like Low-Rank and Sparse Matrix Decomposition (LRaSMD) and Graph and Total Variance Regularized Low-Rank Representation (GTVLRR). These models incorporate sparse coding and structured low-rank constraints to enhance anomaly separation, making them highly effective for HS imagery [166, 35]. Thus, in the separation model, methods have moved from DL to flexible, hybrid models that adopt deep learning components.

The linear reconstruction model. The reconstruction model is the most common anomaly detection strategy and is used for both spectral and spatio-temporal anomaly detection. Essentially, this model uses an explicit DR mapping and its inverse to reconstruct data, identifying anomalies as the samples with high reconstruction error. Simple, variance-preserving linear methods like PCA [79] and a combination of PCA and JPEG-2000 [45] highlight spectral anomalies.

The story of the reconstruction model is similar for spatio-temporal anomalies. DR techniques isolate underlying temporal patterns; for example, a PCA-based anomaly detection approach has helped define extreme weather events across European eco-regions [120]. In SAR data, PCA-based approaches help mitigate speckle and isolate genuine spatial anomalies [47], infrastructure changes [208], and land deformations in SAR data [51]. The

linearity of PCA-based approaches limits their ability to model nonlinear backgrounds, and they perform poorly for more complex anomaly detection tasks.

The nonlinear reconstruction model. Initial steps toward overcoming this complex background challenge include nonlinear variance-preserving DR methods like kPCA. Specifically, kPCA is shown to improve spectral anomaly detection in complex spectral environments [63]. The field quickly moved beyond such methods to adopt more flexible deep learning methods. In this paradigm, many deep learning, AE-based approaches have surfaced [207, 160]. However, standard AEs often generalize too well, reducing the reconstruction error for anomalies [198].

To mitigate this, these methods employ sophisticated regularizers that increase the reconstruction error for anomalies. Sparse and manifold-constrained AEs enforce feature selectivity and preserve local geometric structures, reducing redundant background reconstruction [111]. Transformer-based AEs model long-range dependencies through self-attention, improving feature representation in complex spectral environments [195]. The Regularized Graph AE embeds spatial relationships via superpixel-based regularization to maintain spectral-spatial consistency [50]. Memory-augmented architectures leverage stored background prototypes to suppress anomaly reconstruction, improving contrast [76]. Guided AEs incorporate spectral similarity constraints to reinforce background structure, while fully convolutional networks adjust feature learning dynamically through adaptive loss functions [196, 187].

3.2.3. Predictions

The prediction task often serves as the primary output of RS data analysis. Classical DR for predictions involves reducing the spectral dimension on a pixel-by-pixel basis. Then, DR began to move beyond this narrow view, incorporating contextual information like the spatial distribution of pixels. Recently, DR has been used for representation learning, extracting optimal spectral-spatial-contextual features in an end-to-end pipeline.

Reducing spectral redundancy. The high spectral dimensionality of RS data (especially HS data), combined with the limited number of samples, makes classification challenging due to the redundancy of adjacent bands and pixels. Although PCA is a standard spectral DR method, Harsanyi and Chang’s seminal work built upon it by introducing Orthogonal Subspace Projection (OSP) for simultaneous DR and classification of HS data through enhancing

the signal-to-noise ratio for a desired spectral signature [69]. Other linear matrix factorization DR methods have been used alone or combined to perform DR to improve HS predictions [136]. For example, unsupervised methods, like probabilistic PCA, DWT, and DCuT, and supervised methods like LDA, reduce redundancy and improve classification rates [176, 20, 55, 138, 100]. However, these methods fail to capture nonlinear patterns in the reduced space.

Nonlinear DR methods, specifically manifold learning, capture these complex features through approximating the local structure of the data manifold. For example, injecting local spectral information into LDA reduces HS spectral redundancy, thereby improving classification [101]. MFA also builds upon LDA and was further modified into a DR method called Local Geometric Structure Fisher Analysis (LGSFA), which extracts discriminatory features for improved HS classification by injecting local geometric structures [112]. Hybrid nonlinear DR methods also exist; for example, a combination of Isomap and LLE enhances discrimination among spectrally similar classes compared to traditional methods [8].

Capturing context. Only considering pixel-based information imposes a fundamental ceiling on the predictive performance. To achieve the next step in DR for predictions in RS, researchers looked beyond the single pixel. They incorporated contextual information into DR, thus improving predictive tasks that require understanding spatial relationships, such as object recognition or classification. At first, context was derived from spatial information, then from other sensors, and finally, from different times.

The most immediate form of context is the spatial arrangement of neighboring pixels in a single image. This spatial context was used by Liu et al. to improve object recognition in SAR images by addressing speckle noise image distortion with a locality-preserving algorithm [108]. This context is also encoded directly in the RS data cube. Thus, methods that do not flatten spatial dimensions (e.g., TD) automatically incorporate this structure [86].

Moving beyond single-image context, data fusion can be used as a feature engineering tool to incorporate context from other images and even from different data modalities. For example, fusion competitions evaluate new DR for RS data fusion via landcover classification using the fused reduced features [40, 103, 58]. And case studies on specific DR methods, like supervised MA, use multimodal feature fusion to improve pixel classification rates [175].

Although data fusion incorporates a wide variety of contexts, it misses

the key temporal context of most RS data cubes. DR helps capture temporal information in remote sensing tasks and improve predictive capacity by extracting biophysical variables [146] and handling missing data in time-series [17]. Rivera et al. [146] compare various linear DR methods and their kernel formulations for extracting features to be used as inputs to multivariate regression algorithms. Finally, when restricted to specific frequencies, the DFT can predict NDVI [17].

Even the time dimension is considered by deep learning methods. For example, RS foundation models can take a whole time series of remote sensing images as input and are, as such, especially suitable for dynamic tasks such as change detection. It was shown that this allows building much smaller models with similar performance [173].

Learning the representation. Previous DR methods rely on hand-crafting features. The modern paradigm learns the representation itself, moving from task-specific modes to general-purpose embeddings. Early deep learning methods combine features for a single task. For example, the enhanced hybrid-graph discriminant learning (EHGDL) method builds upon LDA to improve classification accuracy by enhancing class homogeneity and reducing inter-class heterogeneity [113]. Incorporating spatial context, deep learning architectures also improved HS classification [1]. Unsupervised sparse AE is used to fuse LiDAR and optical data, improving maps of forest above-ground biomass [156]. Although these were steps in the right direction for learning reduced representations, they failed to see beyond using features for more than one task.

Beyond autoencoders, deep learning has moved DR into the broader realm of *representation learning* [132]. In this field, the focus shifts from merely reducing dimensions to extracting useful, often equally high-dimensional features that disentangle factors of variation. These rich representations are usually learned through self-supervised learning and can then be applied to various downstream tasks through transfer learning [189].

An important subclass of representation learning is contrastive representation learning. Unlike autoencoders, which are usually trained with a reconstruction loss, these are trained with a contrastive loss [34]. For a similarity function $\text{sim} : \mathcal{Z} \times \mathcal{Z} \rightarrow \mathbb{R}$ (e.g., the cosine similarity) and a positive pair $(\mathbf{z}_i, \mathbf{z}_j) \in \mathcal{Z} \times \mathcal{Z}$ that we want to be similar in the representation (a.k.a.

reduced) space, it is defined by

$$l(\mathbf{z}_i, \mathbf{z}_j) = \log \frac{\exp(\text{sim}(\mathbf{z}_i, \mathbf{z}_j)/\tau)}{\sum_{k=1}^{2N} \mathbb{1}_{[k \neq i]} \exp(\text{sim}(\mathbf{z}_i, \mathbf{z}_k)/\tau)},$$

with $N \in \mathbb{N}_{\geq 1}$ and $\tau > 0$. All other \mathbf{z}_k with $k \in \{1, \dots, 2N\} \setminus \{j\}$ are chosen as negative examples with respect to z_i . This loss essentially encourages representations of datapoints that, in some sense, belong together to be similar, and those of points that do not belong together to be pushed apart.

These contrastive learning approaches are a major turning point because they can learn geographic context without the need for fully labeled datasets, thereby enabling the ingestion of vast archives of unlabeled data. For RS, one forms positive pairs by different augmentations of a scene, e.g., cropped tiles [84] and different seasons [118]. Further extensions include geolocations to ensure that semantically similar nearby images are treated as positive pairs [7]. Satellite contrastive location-image pretraining (SatCLIP), for instance, matches visual patterns in satellite imagery with geographic coordinates. This improves tasks such as temperature prediction and population density estimation [90]. SatCLIP is an example of a general-purpose or foundation model (FM), given its comprehensive self-supervised pre-training and potential applicability to a multitude of downstream tasks.

Nowadays, *Foundation Models* (FMs) produce massive, pretrained, ready-to-use, state-of-the-art embeddings. For example, such self-supervised representation learning techniques, which utilize large neural networks and are trained on vast amounts of data, have been instrumental to the success of large language models (LLMs) for language tasks [210] and are also widely adopted for vision tasks [6]. Different self-supervised learning tasks, such as MAE [168], contrastive learning [53], and self-distillation [183], have emerged as common pretraining tasks, with some studies demonstrating their correspondence to established DR techniques [10].

Such FMs are quickly and enthusiastically being adopted as DR methods to improve RS predictions [110]. Since they can be designed to inject a wide variety of data, they can produce embeddings that capture spatial, multimodal, and temporal context simultaneously. For example, powerful pre-trained representations such as the collection of FM embeddings called Major TOM [38] or the Google Satellite Embedding from the AlphaEarth FM [19] provide readily available, robust features. Multiple benchmarks focus on evaluating the representations provided by foundation models pre-trained for multiple downstream tasks simultaneously, including burn scar,

flood, and crop mapping, land use and land cover classification, and biomass estimation [123].

Although extremely promising, FMs are certainly not the solution for all DR in RS. Firstly, FMs are only as good as their input data, meaning that poor data results in poor FMs. The success of FMs methods over supervised deep learning baselines depends substantially on the resolution, sampling, and modalities of the pre-training data. Overall, FMs are largely black boxes, so embeddings produced by them are generally less interpretable than standard DR methods, leading to a dangerous lack of trustworthiness.

3.3. Synopsis

As we traveled through the uses of DR in the RS data value chain, it has become clear that RS tasks have gone from specific to more general. To support more general, complex tasks, DR methods have moved from linear to nonlinear to extremely general trained embeddings, often obtained by FMs. This begs the question: does traditional DR still have a place in RS? We will address this in Sec. 5.

4. Evaluation metrics for dimensionality reduction

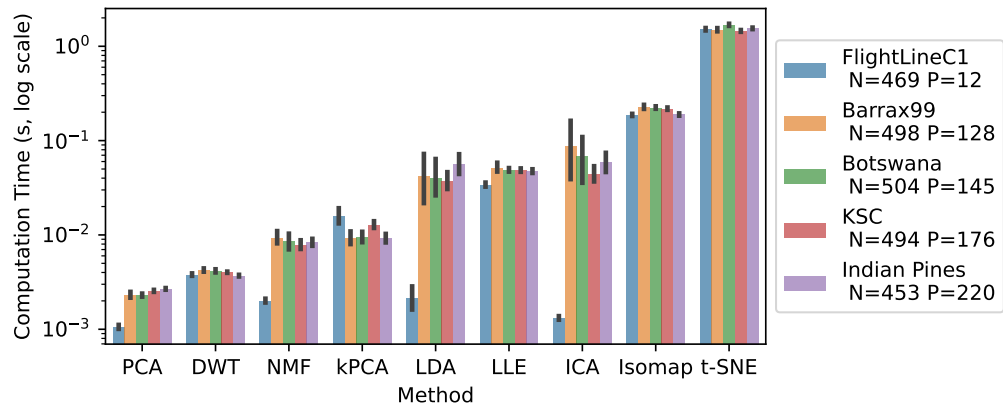


Figure 7: **Computation times for common DR algorithms for different HyperLabelMe datasets [122].** We evaluate unsupervised methods and one supervised method for classification datasets (LDA) to reduce from P to $K = 2$ dimensions. All methods are run on a 2020 MacBook Pro with M1 chip and 16GB of memory.

A common thread through DR in RS is the evaluation of DR methods, an essential step to determining the optimal DR method for a given task. Although DR in RS has evolved, DR evaluation in RS has largely remained the same, as it depends heavily on the downstream RS task. Thus, we provide a collection of the most common metrics from the works surveyed in this review, sorted by RS task in Tab. 2 and an organized bibliography linking each article to its RS task and evaluation metrics in Tab. A.7.

There are two universal metrics: visualization and computation time. Visualization is a useful qualitative metric. For example, suppose a reconstructed image is shifted to the right by one pixel, yielding low correlation and a higher mean squared error with the original image. Still, visually, it might be an acceptable reconstruction that captures the original image’s structure. On the other hand, computation time provides a practical understanding of how quickly DR methods can be executed relative to one another. We compare the computation time of the most common DR methods to reduce the spectrum of various HS images in Fig. 7—the more complex the DR method, the higher the computational cost. Specifically, supervised methods (LDA) are slower than unsupervised methods, and nonlinear methods (kPCA, Isomap, and t-SNE) are slower than linear methods.

Computation time is especially useful for evaluating data compression, where high volumes of data must be quickly reduced. Outside of computation time, evaluation metrics for compression and denoising evaluation metrics compare an original sample $\mathbf{x} \in \mathbb{R}^P$ to its reconstruction $\hat{\mathbf{x}} = \psi \circ \phi(\mathbf{x}) \in \mathbb{R}^P$ to assess reconstruction quality. These metrics assess the reconstruction shape and/or scale and are separated into proxies for similarity (e.g., correlation) and proxies for error (e.g., mean squared error).

Many of the aforementioned metrics are also used to evaluate data fusion. However, in the surveyed works, it was found that specific tools like Universal Image Quality Index (UIQI) [191] and Relative Dimensionless Global Error in Synthesis (ERGAS) [182] are used almost exclusively for evaluating DR for data fusion.

DR for compression, denoising, and fusion are frequently evaluated on the capacity of the reduced or reconstructed data to perform anomaly detection and/ or prediction. Anomaly detection is essentially a binary classification problem and is evaluated by plotting the Receiver Operator Characteristic (ROC) curve and measuring the Area Under the ROC Curve (AUC). Predictions are partitioned into classification and regression, and each is evaluated differently, depending on the data characteristics.

Table 2: **A task-specific guide to evaluation metrics in DR for RS.** This table summarizes the most common metrics, categorized by their purpose and the primary RS task they serve. A table linking RS tasks to evaluation metrics is in Tab. A.7.

RS Task	Metric	What it Measures	Category	Primary Goal
Universal (All Tasks)	Visualization (VIS)	Qualitative assessment of results (e.g., embeddings, reconstructions)	Qualitative	Human interpretation & sanity checks
	Computation Time (CT)	Algorithmic efficiency and resource usage	Quantitative	Assess practical feasibility & scalability
Compression & Denoising	Correlation Coeff. (CC)	Shape similarity between two signals, invariant to scale	Similarity (Shape)	Check pattern/structure preservation
	Signal-to-Noise Ratio (SNR)	Ratio of signal power to noise power	Similarity (Quality)	Assess reconstruction fidelity/scale
	Peak SNR (PSNR)	Distortion relative to the maximum possible signal value	Similarity (Quality)	Standard for reconstruction quality
	Mean Squared Error (MSE)	Average squared magnitude difference between pixels	Error (Magnitude)	Fundamental reconstruction error
	Spectral Angle Dist. (SAD)	Angle between two spectra, invariant to brightness	Error (Shape)	Evaluate spectral signature fidelity
Data Fusion	Rate Distortion (RD/BR)	Curve of reconstruction quality vs. compression level (bit rate)	Performance Curve	Compare algorithm compression efficiency
	ERGAS	Relative global error, assessing radiometric and spectral quality	Error (Global Quality)	Standardized quality score for fused products
	UIQI	Combination of structural, luminance, and contrast similarity	Similarity (Structural)	Assess perceptual/visual quality of fusion
Anomaly Detection	ROC / AUC	Trade-off between true positive rate and false positive rate	Classification Perf.	Evaluate detection sensitivity vs. false alarms
Predictions	Accuracy (ACC)	Overall percentage of correct classifications	Classification Perf.	Simple baseline (can mislead on imbalanced data)
	F1-score / Cohen's Kappa (κ)	Metrics robust to class imbalance (precision/recall, agreement)	Classification Perf.	Robust evaluation of classifier performance
	R-squared (R^2)	Proportion of variance in the target variable explained by the model	Regression Perf.	Evaluate regression model fit and performance

4.1. Synopsis

Evaluation of DR in the RS data value chain is highly task-specific. So, either there is a need for metrics for general DR evaluation in RS, or we must accept that there is no sufficiently general DR evaluation method for all RS tasks.

5. Trends and perspectives

Across the data value chain, we observe that earlier works began using linear unsupervised methods, such as PCA, for DR. Recently, DR in RS has shifted towards deep learning and foundation models for complex, nonlinear, and general features. We outline this paradigm shift in Sec. 5.1. Then, we identify three perspectives on DR in this new era, arising from trends extracted from our survey. Specifically, we identify a bridge between deep learning and classical DR in Sec. 5.2, and then we emphasize the need for interpretable embeddings in Sec. 5.3. A glossary of the DR methods discussed in this section is in Tab. 3.

5.1. From single-task models to unified representations

Deep learning for specific tasks and simple multimodal fusion are becoming the state-of-the-art for learning joint representations of RS data. This trend points toward a grander future carried on the shoulders of large-scale, multi-modal Foundation Models (FMs) that may provide the ultimate unification of RS data.

Standard methods for RS compression, like JPEG-2000 are multi-step pipelines that include DR, like the DWT. JPEG-AI outperforms JPEG-2000 and unifies data compression into a single step using advances in deep learning [5]. Although JPEG-AI remains largely untested in RS, deep learning-based compression methods for Earth observation, such as TerraCodec [37], are already revolutionizing RS data compression.

Deep learning methods have been adapted to a wide range of data structures, such as images, time series, and graphs. They are thus a clear candidate for a structure that can unify different modalities of RS. Contrastive learning leverages pairings of different modalities [53], and Masked Autoencoders (MAE) reconstruct masked modalities from the remaining ones to learn joint representations [168]. This can be seen as an implicit form of fusion.

The goal of FMs is to bring this unification to its final form, aiming to integrate as many modalities as possible, which could eventually even lead to a fusion of RS, climate, weather, and in-situ data [212]. Recent FMs integrate, for instance, SAR with optical satellite imagery [200] and use diffusion to generate missing modalities from the unified representation [80].

Table 3: **Perspective DR methods for RS.** These methods are organized by our three perspectives for DR in RS.

Perspective	Abbreviation	Method	Ref
From single-task models to unified representations	CL	Contrastive Learning	[53]
	AlphaEarth	Google Satellite Embedding	[19]
	JPEG-AI	JPEG-AI	[5]
	MAE	Masked Autoencoder	[168]
	Major-TOM	Terrestrial Observation Metaset	[38]
	MoCo	Momentum Contrast	[84]
	Sat-CLIP	Satellite Contrastive Location-Image Pretraining	[90]
	SD	Self-distillation	[183]
	TEC	TerraCodec	[37]
Bridging classical DR and modern representation learning	UMAP	Uniform Manifold Approximation and Projection	[125]
	NOMAD	Negative or mean affinity discrimination	[48]
	t-SimCNE	t-SimCNE	[16]
The rise of black boxes and the need for robustness and interpretability	CFL	Causal Feature Learning	[29]
	DPCP	Dual PC Pursuit	[172]
	EHGDL	Enhanced Hybrid-Graph Discriminant Learning	[113]
	gPCA	Granger Principal Component Analysis	[180]
	LGSFA	Local Geometric Structure Fisher Analysis	[112]
	PAA	Piecewise Aggregate Approximation	[87]
	PSA	Principal Subspace Analysis	[167]
	RSR	Robust Subspace Recovery	[96]
	TeACFNet	Texture-Aware Causal Feature Extraction Network	[202]

Despite their promise, the deep learning-derived representations of FMs have not yet fully lived up to expectations in RS applications [142]. They are often beaten by standard deep-learning baselines in segmentation or regression tasks [123], which can be attributed to a mismatch in resolution and modalities or poor sampling of the pre-training data. Recent work has developed a mechanism using FMs for RS to flag potential failures in advance [36]. However, the question of why these failures exits, remains open and a promising avenue for future research.

5.2. Bridging classical DR and modern representation learning

Another issue with FM embeddings is that we no longer struggle with the raw sensor dimensions; we struggle to understand and interpret the complex, high-dimensional embeddings produced by these models. Thus, FMs essentially trade the original raw RS dimensionality problem with another. Luckily, we suggest addressing this issue via bridging classical DR with modern representation learning. We propose two bridges: one that uses classical DR on FM embeddings, and a second bridge for the development of hybrid classical DR-FM methods.

DR can be used to interpret FM embeddings and provide task-specific representations when such embeddings are too general. These roles are most evident in visualization, where methods such as t-SNE have already been applied to feature spaces of deep learning models [209, 150]. Other nonlinear topology-preserving DR methods, such as Uniform Manifold Approximation and Projection (UMAP), can also be used to explore these latent spaces [125]. Recently, an accelerated version of t-SNE, negative or mean affinity discrimination (NOMAD) projection [48], enables the visualization of extremely large-scale RS datasets and FM embeddings.

Two glaring limitations of these t-SNE and UMAP are that they are computationally expensive and implicit, meaning they cannot be applied to test data or produce data reconstructions. In general, DR families like manifold learning suffer from implicit DR mappings, meaning that these methods are not readily transferable to test or out-of-distribution datasets. To remedy this issue, we consider a simple yet ambitious framework for reformulating implicit DR mappings as explicit. Specifically, we propose hybrid DR methods that exchange optimizing for a reduced space embedding with optimizing for neural network parameters to explicitly map to the embedding. Damrich et al. explored this concept with t-SNE and UMAP, finding that both can be formulated as explicit DR [39]. Another perspective of hybrid DR-FM

methods is a variant of t-SNE called t-SimCNE [16]. Research continuing in this direction will certainly produce more scalable and interpretable visualizations of large-scale RS datasets, facilitating exploratory analysis and downstream applications.

5.3. The Rise of Black Boxes and the Need for Robustness and Interpretability

The pursuit of performance with black box models has created two critical failures: a lack of robustness to imperfect data and a lack of scientific interpretability. With the rise of deep learning and FMs, we gain in generalizability but lose in robustness and interpretability.

Going back to the basics with simple, robust, and principled variations of PCA that are still under-explored on RS datasets may improve both denoising and anomaly detection. For example, Robust PCA [28], applied for foreground/background separation, shows potential for both denoising with outlier-contaminated data and anomaly detection. Furthermore, Robust subspace recovery [96] and dual principal component pursuit [172] are used for outlier rejection and robust model fitting in computer vision, and almost not been tested in RS.

The next step in this challenge is to assess the scientific interpretability of these principal components. Recently, a curse of isotropy has been uncovered in PCA, indicating that often PCs should be grouped into principal subspaces [167]. This means that single principal components from PCA used in climate science as proxies for climate indices (e.g., ENSO) may oversimplify complex climate variability. Rotating a single vector in this subspace to align with the physical process enables more interpretable modes of variability compared to those derived from a single principal component.

Moving beyond interpretability, we would ideally arrive at a causal understanding of these reduced dimensions. FMs and traditional DR methods alike fail to separate causal features from spurious correlations, limiting generalization under domain shifts, compromising robustness and explainability [174]. Causality-aware DR methods address this by disentangling actual signals from biases, thereby ensuring robust and transferable representations [22]. In applications, this makes RS tasks, such as prediction, more robust and improves generalization. For example, linear causality-aware DR adapts PCA to detect Granger causal directions via Granger PCA (gPCA) [180]. Furthermore, deep learning DR has been injected with causal reasoning resulting in methods like Causal Feature Learning (CFL) [29] and Texture-Aware Causal

Feature Extraction Network (TeACFNet) [202]. Using these methods, we can detect causal features that improve the generalization of RS models under domain shifts (e.g., climate change and data from new sensors).

5.4. *Synopsis*

Although FMs show promise as a large general DR, their embeddings are often still high-dimensional, and their black box nature makes them difficult to interpret. In the future, DR in RS will remain task-specific by using DR on FM embeddings, building hybrid DR-FM methods, and advancing the use of robust, interpretable, and potentially causal DR methods in RS.

6. Conclusions

After providing a framework of standard DR methods in RS, we have traversed the entire RS data value chain and exposed the current utility of DR for each challenge. This voyage revealed the shift in DR in RS from unsupervised linear methods to the foundation-model era. As researchers facing this bold new paradigm, there is a real possibility of unifying all RS data into a cohesive representation. However, these general FM embeddings risk scientific opacity by prioritizing benchmark performance over physical structure, and potentially decouple RS models from true physical meaning. Thus, we conclude with three claims: FM embeddings are not sufficient for RS science, classical DR is not obsolete in RS, but complementary to FMs, and finally, robustness and interpretability are essential pillars of DR for RS.

In summary, we posit that the FM era should not be a full replacement of classical DR, but a reconfiguration, a synergistic incorporation of classical DR with modern foundation models. DR for RS should focus on building hybrid pipelines that couple standard DR with FMs for extracting compact, task-relevant features. This direction is necessary to achieve more efficient, trustworthy, and explainable feature representations of Earth system data.

Acknowledgements

N.M. and G.C-V. acknowledge the support of Generalitat València and the Conselleria d’Innovació, Universitats, Ciéncia i Societat Digital, through the project “AI4CS: Artificial Intelligence for complex systems: Brain, Earth, Climate, Society” (CIPROM/2021/56). K-H. C. & G.C-V. acknowledge the support from the European Research Council (ERC) under the ERC Synergy

Grant USMILE (grant agreement 855187). G.C-V. acknowledges the support from the HORIZON program under the AI4PEX project (grant agreement 101137682).

References

- [1] Abdi, G., Samadzadegan, F., Reinartz, P., 2017. Spectral-spatial feature learning for hyperspectral imagery classification using deep stacked sparse autoencoder. *Journal of Applied Remote Sensing* 11, 042604–042604.
- [2] Ahmed, N., Natarajan, T., Rao, K.R., 1974. Discrete cosine transform. *IEEE Transactions on Computers* 100, 90–93.
- [3] Akaho, S., 2006. A kernel method for canonical correlation analysis. *arXiv preprint cs/0609071* .
- [4] Altman, N., Krzywinski, M., 2018. The curse(s) of dimensionality. *Nature Methods* 15, 399–400.
- [5] Ascenso, J., Alshina, E., Ebrahimi, T., 2023. The jpeg ai standard: Providing efficient human and machine visual data consumption. *Ieee Multimedia* 30, 100–111.
- [6] Awais, M., Naseer, M., Khan, S., Anwer, R.M., Cholakkal, H., Shah, M., Yang, M.H., Khan, F.S., 2025. Foundation models defining a new era in vision: A survey and outlook. *IEEE Transactions on Pattern Analysis and Machine Intelligence* 47, 2245–2264. doi:10.1109/TPAMI.2024.3506283.
- [7] Ayush, K., Uzkent, B., Meng, C., Tanmay, K., Burke, M., Lobell, D., Ermon, S., 2021. Geography-aware self-supervised learning, in: *Proceedings of the IEEE/CVF International Conference on Computer Vision (ICCV)*, pp. 10181–10190.
- [8] Bachmann, C.M., Ainsworth, T.L., Fusina, R.A., 2005. Exploiting manifold geometry in hyperspectral imagery. *IEEE transactions on Geoscience and Remote Sensing* 43, 441–454.
- [9] Balasubramanian, M., Schwartz, E.L., 2002. The isomap algorithm and topological stability. *Science* 295, 7–7.
- [10] Balestriero, R., LeCun, Y., 2022. Contrastive and non-contrastive self-supervised learning recover global and local spectral embedding methods, in: Oh, A.H., Agarwal, A., Belgrave, D., Cho, K. (Eds.),

Advances in Neural Information Processing Systems. URL: <https://openreview.net/forum?id=jQgsZDspz5h>.

- [11] Bandos, T.V., Bruzzone, L., Camps-Valls, G., 2009. Classification of hyperspectral images with regularized linear discriminant analysis. *IEEE Transactions on Geoscience and Remote Sensing* 47, 862–873.
- [12] Bank, D., Koenigstein, N., Giryes, R., 2023. Autoencoders. *Machine Learning for Data Science Handbook: Data Mining and Knowledge Discovery Handbook* , 353–374.
- [13] Barnston, A.G., Livezey, R.E., 1987. Classification, seasonality and persistence of low-frequency atmospheric circulation patterns. *Monthly Weather Review* 115, 1083–1126. URL: https://journals.ametsoc.org/view/journals/mwre/115/6/1520-0493_1987_115_1083_csapol_2_0_co_2.xml, doi:10.1175/1520-0493(1987)115<1083:CSAPOL>2.0.CO;2.
- [14] Baudat, G., Anouar, F., 2000. Generalized discriminant analysis using a kernel approach. *Neural computation* 12, 2385–2404.
- [15] Benz, U., Strobl, K., Moreira, A., 1995. A comparison of several algorithms for SAR raw data compression. *IEEE Transactions on Geoscience and Remote Sensing* 33, 1266–1276.
- [16] Böhm, N., Berens, P., Kobak, D., 2023. Unsupervised visualization of image datasets using contrastive learning, in: *The Eleventh International Conference on Learning Representations*. URL: <https://openreview.net/forum?id=nI2HmVA0hvt>.
- [17] Brooks, E.B., Thomas, V.A., Wynne, R.H., Coulston, J.W., 2012. Fitting the multitemporal curve: A Fourier series approach to the missing data problem in remote sensing analysis. *IEEE Transactions on Geoscience and Remote Sensing* 50, 3340–3353.
- [18] Broughton, S.A., Bryan, K., 2018. *Discrete Fourier analysis and wavelets: applications to signal and image processing*. John Wiley & Sons.
- [19] Brown, C.F., Kazmierski, M.R., Pasquarella, V.J., Rucklidge, W.J., Samsikova, M., Zhang, C., Shelhamer, E., Lahera, E., Wiles, O.,

Ilyushchenko, S., et al., 2025. AlphaEarth Foundations: An embedding field model for accurate and efficient global mapping from sparse label data. arXiv preprint arXiv:2507.22291 .

[20] Bruce, L., Koger, C., Li, J., 2002. Dimensionality reduction of hyperspectral data using discrete wavelet transform feature extraction. *IEEE Transactions on Geoscience and Remote Sensing* 40, 2331–2338. doi:10.1109/TGRS.2002.804721.

[21] Bueso, D., Piles, M., Camps-Valls, G., 2020. Nonlinear PCA for spatio-temporal analysis of Earth observation data. *IEEE Transactions on Geoscience and Remote Sensing* 58, 5752–5763.

[22] Bühlmann, P., 2020. Invariance, causality and robustness. *Statistical Science* 35, 404–426.

[23] Camps-Valls, G., Bruzzone, L., 2009a. Kernel methods for remote sensing data analysis. John Wiley & Sons.

[24] Camps-Valls, G., Bruzzone, L. (Eds.), 2009b. Kernel methods for remote sensing data analysis. Wiley & Sons, UK.

[25] Camps-Valls, G., Tuia, D., Zhu, X., Reichstein, M.E., 2021. Deep learning for the Earth Sciences: A comprehensive approach to remote sensing, climate science and geosciences. Wiley & Sons. URL: <https://github.com/DL4ES>.

[26] Canas, A.A.D., Barnett, M.E., 1985. The generation and interpretation of false-colour composite principal component images. *International Journal of Remote Sensing* 6, 867–881. URL: <https://doi.org/10.1080/01431168508948510>, doi:10.1080/01431168508948510, arXiv:<https://doi.org/10.1080/01431168508948510>.

[27] Candes, E.J., Donoho, D.L., et al., 1999. Curvelets: A surprisingly effective nonadaptive representation for objects with edges. Department of Statistics, Stanford University Stanford, CA, USA.

[28] Candès, E.J., Li, X., Ma, Y., Wright, J., 2011. Robust principal component analysis? *Journal of the ACM (JACM)* 58, 1–37.

- [29] Chalupka, K., Eberhardt, F., Perona, P., 2017. Causal feature learning: An overview. *Behaviormetrika* 44, 137–164.
- [30] Chandola, V., Banerjee, A., Kumar, V., 2009. Anomaly detection: A survey. *ACM Computing Surveys* 41. URL: <https://doi.org/10.1145/1541880.1541882>, doi:10.1145/1541880.1541882.
- [31] Chatterjee, A., 2000. An introduction to the proper orthogonal decomposition. *Current science* , 808–817.
- [32] Chavez, Jr, P., Sides, S., Anderson, J., 1991. Comparison of three different methods to merge multiresolution and multispectral data: Landsat tm and spot panchromatic. *Photogrammetric Engineering and Remote Sensing* 57, 265–303.
- [33] Chen, G., Qian, S.E., 2010. Denoising of hyperspectral imagery using principal component analysis and wavelet shrinkage. *IEEE Transactions on Geoscience and remote sensing* 49, 973–980.
- [34] Chen, T., Kornblith, S., Norouzi, M., Hinton, G., 2020. A simple framework for contrastive learning of visual representations, in: *Proceedings of the 37th International Conference on Machine Learning*, JMLR.org.
- [35] Cheng, T., Wang, B., 2020. Graph and total variation regularized low-rank representation for hyperspectral anomaly detection. *IEEE Transactions on Geoscience and Remote Sensing* 58, 391–406. doi:10.1109/TGRS.2019.2936609.
- [36] Cohrs, K.H., Osika, Z., Gonzalez-Calabuig, M., Nedungadi, V., Cartuyvels, R., Knoblauch, S., Massant, J., Nath, S., Ebel, P., Sitokonstantinou, V., 2025. Shrug-fm: Reliability-aware foundation models for earth observation. URL: <https://arxiv.org/abs/2511.10370>, arXiv:2511.10370.
- [37] Costa-Watanabe, J., Wittmann, I., Blumenstiel, B., Schindler, K., 2025. TerraCodec: Compressing Earth observations. arXiv preprint arXiv:2510.12670 .
- [38] Czerkawski, M., Kluczek, M., Bojanowski, J.S., 2024. Global and dense embeddings of Earth: Major TOM floating in the latent space. URL: <https://arxiv.org/abs/2412.05600>, arXiv:2412.05600.

- [39] Damrich, S., Böhm, J.N., Hamprecht, F.A., Kobak, D., 2022. From t-SNE to UMAP with contrastive learning. arXiv preprint arXiv:2206.01816 .
- [40] Debes, C., Merentitis, A., Heremans, R., Hahn, J.T., Frangiadakis, N., van Kasteren, T., Liao, W., Bellens, R., Pivzurica, A., Gautama, S., Philips, W., Prasad, S., Du, Q., Pacifici, F., 2014. Hyperspectral and LiDAR data fusion: Outcome of the 2013 grss data fusion contest. IEEE Journal of Selected Topics in Applied Earth Observations and Remote Sensing 7, 2405–2418. URL: <https://api.semanticscholar.org/CorpusID:18245569>.
- [41] Dey, N., Bhatt, C., Ashour, A.S., 2018. Big data for remote sensing: Visualization, analysis and interpretation. Cham: Springer 104.
- [42] Ding, H., Xie, F., Qiu, L., Zhang, X., Shi, Z., 2024. Robust haze and thin cloud removal via conditional variational autoencoders. IEEE Transactions on Geoscience and Remote Sensing .
- [43] Dong, J., Yin, R., Sun, X., Li, Q., Yang, Y., Qin, X., 2018. Inpainting of remote sensing SST images with deep convolutional generative adversarial network. IEEE Geoscience and Remote Sensing Letters 16, 173–177.
- [44] Du, B., Zhang, L., 2014. A discriminative metric learning based anomaly detection method. IEEE Transactions on Geoscience and Remote Sensing 52, 6844–6857. doi:10.1109/TGRS.2014.2303895.
- [45] Du, Q., Fowler, J.E., 2007. Hyperspectral image compression using JPEG2000 and principal component analysis. IEEE Geoscience and Remote Sensing Letters 4, 201–205. doi:10.1109/LGRS.2006.888109.
- [46] Dua, Y., Kumar, V., Singh, R.S., 2020. Comprehensive review of hyperspectral image compression algorithms. Optical Engineering 59, 090902–090902.
- [47] Duan, Y., Yang, C., Chen, H., Yan, W., Li, H., 2021. Low-complexity point cloud denoising for LiDAR by PCA-based dimension reduction. Optics Communications 482, 126567.

- [48] Duderstadt, B., Nussbaum, Z., Van der Maaten, L., 2025. NOMAD projection. arXiv preprint arXiv:2505.15511 .
- [49] Duhamel, P., Vetterli, M., 1990. Fast Fourier transforms: A tutorial review and a state of the art. *Signal processing* 19, 259–299.
- [50] Fan, G., Ma, Y., Mei, X., Fan, F., Huang, J., Ma, J., 2021. Hyperspectral anomaly detection with robust graph autoencoders. *IEEE Transactions on Geoscience and Remote Sensing* 60, 1–15. doi:10.1109/TGRS.2021.3097097.
- [51] Festa, D., Novellino, A., Hussain, E., Bateson, L., Casagli, N., Confuerto, P., Del Soldato, M., Raspini, F., 2023. Unsupervised detection of InSAR time series patterns based on PCA and k-means clustering. *International Journal of Applied Earth Observation and Geoinformation* 118, 103276. URL: <https://www.sciencedirect.com/science/article/pii/S1569843223000985>, doi:<https://doi.org/10.1016/j.jag.2023.103276>.
- [52] Flach, M., Gans, F., Brenning, A., Denzler, J., Reichstein, M., Rodner, E., Bathiany, S., Bodesheim, P., Guanche, Y., Sippel, S., Mahecha, M.D., 2017. Multivariate anomaly detection for Earth observations: A comparison of algorithms and feature extraction techniques. *Earth System Dynamics* 8, 677–696. URL: <https://esd.copernicus.org/articles/8/677/2017/>, doi:10.5194/esd-8-677-2017.
- [53] Fuller, A., Millard, K., Green, J.R., 2023. CROMA: Remote sensing representations with contrastive radar-optical masked autoencoders, in: Thirty-seventh Conference on Neural Information Processing Systems. URL: <https://openreview.net/forum?id=ezqI5WgGvY>.
- [54] Garcia-Sobrino, J., Laparra, V., Serra-Sagristà, J., Calbet, X., Camps-Valls, G., 2019. Improved statistically based retrievals via spatial-spectral data compression for IASI data. *IEEE Transactions on Geoscience and Remote Sensing* 57, 5651–5668.
- [55] García-Sobrino, J., Serra-Sagristà, J., Laparra, V., Calbet, X., Camps-Valls, G., 2017. Statistical atmospheric parameter retrieval largely benefits from spatial-spectral image compression. *IEEE Transactions on Geoscience and Remote Sensing* 55, 2213–2224.

[56] García-Vilchez, F., Muñoz Marí, J., Zortea, M., Blanes, I., González-Ruiz, V., Camps-Valls, G., Plaza, A., Serra-Sagristà, J., 2011. On the impact of lossy compression on hyperspectral image classification and unmixing. *IEEE Geoscience and Remote Sensing Letters* 8, 253–257. doi:10.1109/LGRS.2010.2062484.

[57] Geladi, P., Kowalski, B.R., 1986. Partial least-squares regression: A tutorial. *Analytica chimica acta* 185, 1–17.

[58] Ghamisi, P., Höfle, B., Zhu, X.X., 2017. Hyperspectral and LiDAR data fusion using extinction profiles and deep convolutional neural network. *IEEE Journal of Selected Topics in Applied Earth Observations and Remote Sensing* 10, 3011–3024. doi:10.1109/JSTARS.2016.2634863.

[59] Ghamsi, P., Rasti, B., Yokoya, N., Wang, Q., Hofle, B., Bruzzone, L., Bovolo, F., Chi, M., Anders, K., Gloaguen, R., Atkinson, P.M., Benediktsson, J.A., 2019. Multisource and multitemporal data fusion in remote sensing: A comprehensive review of the state of the art. *IEEE Geoscience and Remote Sensing Magazine* 7, 6–39. doi:10.1109/MGRS.2018.2890023.

[60] Goodman, S.J., 2020. GOES-R series introduction, in: *The GOES-R Series*. Elsevier, pp. 1–3.

[61] Green, A.A., Berman, M., Switzer, P., Craig, M.D., 1988. A transformation for ordering multispectral data in terms of image quality with implications for noise removal. *IEEE Transactions on Geoscience and Remote Sensing* 26, 65–74.

[62] Gross, M.H., Seibert, F., 1993. Visualization of multidimensional image data sets using a neural network. *The Visual Computer* 10, 145–159.

[63] Gu, Y., Liu, Y., Zhang, Y., 2008. A selective KPCA algorithm based on high-order statistics for anomaly detection in hyperspectral imagery. *IEEE Geoscience and Remote Sensing Letters* 5, 43–47. doi:10.1109/LGRS.2007.907304.

[64] Gupta, D., Golder, A., Zhu, R., Cui, K., Tang, W., Yang, F., Csillik, O., Alaqahtani, S., Pauca, V.P., 2025. Mosaic: Multi-modal multi-label supervision-aware contrastive learning for remote sensing. URL: <https://arxiv.org/abs/2507.08683>, arXiv:2507.08683.

- [65] Haenlein, M., Kaplan, A.M., 2004. A beginner's guide to partial least squares analysis. *Understanding statistics* 3, 283–297.
- [66] Ham, J., Lee, D., Saul, L., 2005. Semisupervised alignment of manifolds, in: International Workshop on Artificial Intelligence and Statistics, PMLR. pp. 120–127.
- [67] Hannachi, A., Jolliffe, I.T., Stephenson, D.B., 2007. Empirical Orthogonal Functions and related techniques in atmospheric science: A review. *International Journal of Climatology* 27, 1119–1152.
- [68] Hao, X., Liu, L., Yang, R., Yin, L., Zhang, L., Li, X., 2023. A review of data augmentation methods of remote sensing image target recognition. *Remote Sensing* 15, 827.
- [69] Harsanyi, J., Chang, C.I., 1994. Hyperspectral image classification and dimensionality reduction: an orthogonal subspace projection approach. *IEEE Transactions on Geoscience and Remote Sensing* 32, 779–785. doi:10.1109/36.298007.
- [70] Horel, J.D., 1984. Complex principal component analysis: Theory and examples. *Journal of Applied Meteorology and Climatology* 23, 1660–1673.
- [71] Horel, J.D., Wallace, J.M., 1981. Planetary-scale atmospheric phenomena associated with the Southern Oscillation. *Monthly Weather Review* 109, 813–829. URL: https://journals.ametsoc.org/view/journals/mwre/109/4/1520-0493_1981_109_0813_psapaw_2_0_co_2.xml; doi:10.1175/1520-0493(1981)109<0813:PSAPAW>2.0.CO;2.
- [72] Hotelling, H., 1933. Analysis of a complex of statistical variables into principal components. *Journal of educational psychology* 24, 417.
- [73] Hu, X., Xie, C., Fan, Z., Duan, Q., Zhang, D., Jiang, L., Wei, X., Hong, D., Li, G., Zeng, X., et al., 2022. Hyperspectral anomaly detection using deep learning: A review. *Remote Sensing* 14, 1973.
- [74] Huang, W., Fei, X., Feng, J., Wang, H., Liu, Y., Huang, Y., 2020. Pan-sharpening via multi-scale and multiple deep neural networks. *Signal Processing: Image Communication* 85, 115850. URL: <https://www.sciencedirect.com/science/article/>

pii/S0923596520300710, doi:<https://doi.org/10.1016/j.image.2020.115850>.

- [75] Huang, W., Xiao, L., Wei, Z., Liu, H., Tang, S., 2015. A new pan-sharpening method with deep neural networks. *IEEE Geoscience and Remote Sensing Letters* 12, 1037–1041. doi:[10.1109/LGRS.2014.2376034](https://doi.org/10.1109/LGRS.2014.2376034).
- [76] Huo, Y., Cheng, X., Lin, S., Zhang, M., Wang, H., 2024. Memory-augmented autoencoder with adaptive reconstruction and sample attribution mining for hyperspectral anomaly detection. *IEEE Transactions on Geoscience and Remote Sensing* 62, 99313–99325. doi:[10.1109/TGRS.2024.3399313](https://doi.org/10.1109/TGRS.2024.3399313).
- [77] Ibebuchi, C., 2024. Redefining the North Atlantic Oscillation index generation using autoencoder neural network. *Machine Learning- Science and Technology* doi:[10.1088/2632-2153/ad1c32](https://doi.org/10.1088/2632-2153/ad1c32).
- [78] Izquierdo-Verdiguier, E., Laparra, V., Marí, J.M., Chova, L.G., Camps-Valls, G., 2017. Advanced feature extraction for Earth observation data processing, in: *Comprehensive remote sensing*, volume 2: data processing and analysis methodology. Elsevier, pp. 108–133.
- [79] Jablonski, J.A., Bihl, T.J., Bauer, K.W., 2015. Principal component reconstruction error for hyperspectral anomaly detection. *IEEE Geoscience and Remote Sensing Letters* 12, 1725–1729. doi:[10.1109/LGRS.2015.2421813](https://doi.org/10.1109/LGRS.2015.2421813).
- [80] Jakubik, J., Yang, F., Blumenstiel, B., Scheurer, E., Sedona, R., Maurogiovanni, S., Bosmans, J., Dionelis, N., Marsocci, V., Kopp, N., Ramachandran, R., Fraccaro, P., Brunschwiler, T., Cavallaro, G., Bernabe-Moreno, J., Longépé, N., 2025. TerraMind: Large-scale generative multimodality for Earth observation. URL: <https://arxiv.org/abs/2504.11171>, arXiv:2504.11171.
- [81] Jutten, C., Herault, J., 1991. Blind separation of sources, part i: An adaptive algorithm based on neuromimetic architecture. *Signal processing* 24, 1–10.

[82] Kaarna, A., Zemcik, P., Kalviainen, H., Parkkinen, J., 2000. Compression of multispectral remote sensing images using clustering and spectral reduction. *IEEE transactions on Geoscience and Remote Sensing* 38, 1073–1082.

[83] Kandasamy, S., Baret, F., Verger, A., Neveux, P., Weiss, M., 2013. A comparison of methods for smoothing and gap filling time series of remote sensing observations—application to MODIS LAI products. *Biogeosciences* 10, 4055–4071.

[84] Kang, J., Fernandez-Beltran, R., Duan, P., Liu, S., Plaza, A.J., 2021a. Deep unsupervised embedding for remotely sensed images based on spatially augmented momentum contrast. *IEEE Transactions on Geoscience and Remote Sensing* 59, 2598–2610. doi:10.1109/TGRS.2020.3007029.

[85] Kang, L., Hu, X., Zhong, C., Zhang, K., Jiang, Y., 2021b. Comparative study of different dimensionality reduction methods in hyperspectral image classification. *Journal of Physics: Conference Series* 2024, 012009. URL: <https://dx.doi.org/10.1088/1742-6596/2024/1/012009>, doi:10.1088/1742-6596/2024/1/012009.

[86] Karami, A., Yazdi, M., Mercier, G., 2012. Compression of hyperspectral images using discrete wavelet transform and tucker decomposition. *IEEE Journal of Selected Topics in Applied Earth Observations and Remote Sensing* 5, 444–450. doi:10.1109/JSTARS.2012.2189200.

[87] Keogh, E., Chakrabarti, K., Pazzani, M., Mehrotra, S., 2001. Dimensionality reduction for fast similarity search in large time series databases. *Knowledge and Information Systems* 3, 263–286.

[88] Kingma, D.P., Welling, M., 2013. Auto-encoding variational bayes. arXiv preprint arXiv:1312.6114 .

[89] Kingra, P.K., Majumder, D., Singh, S.P., 2016. Application of remote sensing and GIS in agriculture and natural resource management under changing climatic conditions. *Agricultural Research Journal* 53.

[90] Klemmer, K., Rolf, E., Robinson, C., Mackey, L., Rußwurm, M., 2023. SatCLIP: Global, general-purpose location embeddings with satellite imagery. arXiv preprint arXiv:2311.17179 .

- [91] Kobak, D., Linderman, G.C., 2021. Initialization is critical for preserving global data structure in both t-sne and umap. *Nature biotechnology* 39, 156–157.
- [92] Kohonen, T., 1990. The self-organizing map. *Proceedings of the IEEE* 78, 1464–1480.
- [93] Kreutz-Delgado, K., Murray, J.F., Rao, B.D., Engan, K., Lee, T.W., Sejnowski, T.J., 2003. Dictionary learning algorithms for sparse representation. *Neural computation* 15, 349–396.
- [94] Lalitha, V., Latha, B., 2022. A review on remote sensing imagery augmentation using deep learning. *Materials Today: Proceedings* 62, 4772–4778.
- [95] Lee, J.A., Verleysen, M., 2007. Nonlinear dimensionality reduction. Springer Science & Business Media.
- [96] Lerman, G., Maunu, T., 2018. An overview of robust subspace recovery. *Proceedings of the IEEE* 106, 1380–1410.
- [97] Li, H., Cui, J., Zhang, X., Han, Y., Cao, L., 2022a. Dimensionality reduction and classification of hyperspectral remote sensing image feature extraction. *Remote Sensing* 14, 4579.
- [98] Li, J., Hong, D., Gao, L., Yao, J., Zheng, K., Zhang, B., Chanussot, J., 2022b. Deep learning in multimodal remote sensing data fusion: A comprehensive review. *International Journal of Applied Earth Observation and Geoinformation* 112, 102926.
- [99] Li, J., Pei, Y., Zhao, S., Xiao, R., Sang, X., Zhang, C., 2020. A review of remote sensing for environmental monitoring in China. *Remote Sensing* 12, 1130.
- [100] Li, W., Feng, F., Li, H., Du, Q., 2018. Discriminant analysis-based dimension reduction for hyperspectral image classification: A survey of the most recent advances and an experimental comparison of different techniques. *IEEE Geoscience and Remote Sensing Magazine* 6, 15–34.
- [101] Li, W., Prasad, S., Fowler, J.E., Bruce, L.M., 2011. Locality-preserving dimensionality reduction and classification for hyperspectral image

analysis. *IEEE Transactions on Geoscience and Remote Sensing* 50, 1185–1198.

- [102] Li, X., Wang, L., Cheng, Q., Wu, P., Gan, W., Fang, L., 2019. Cloud removal in remote sensing images using nonnegative matrix factorization and error correction. *ISPRS Journal of Photogrammetry and Remote Sensing* 148, 103–113.
- [103] Liao, W., Huang, X., Van Coillie, F., Gautama, S., Pižurica, A., Philips, W., Liu, H., Zhu, T., Shimoni, M., Moser, G., Tuia, D., 2015. Processing of multiresolution thermal hyperspectral and digital color data: Outcome of the 2014 IEEE GRSS data fusion contest. *IEEE Journal of Selected Topics in Applied Earth Observations and Remote Sensing* 8, 2984–2996. doi:10.1109/JSTARS.2015.2420582.
- [104] Liu, C., Ray, S., Hooker, G., Friedl, M., 2012a. Functional factor analysis for periodic remote sensing data. *The Annals of Applied Statistics* 6, 601–624.
- [105] Liu, C., Zhang, Y., Wang, S., Sun, M., Ou, Y., Wan, Y., Liu, X., 2020. Band-independent encoder–decoder network for pan-sharpening of remote sensing images. *IEEE Transactions on Geoscience and Remote Sensing* 58, 5208–5223. doi:10.1109/TGRS.2020.2975230.
- [106] Liu, G., Li, L., Jiao, L., Dong, Y., Li, X., 2019. Stacked Fisher autoencoder for SAR change detection. *Pattern Recognition* 96, 106971. URL: <https://www.sciencedirect.com/science/article/pii/S0031320319302742>, doi:<https://doi.org/10.1016/j.patcog.2019.106971>.
- [107] Liu, H., Yang, J., Ye, M., James, S.C., Tang, Z., Dong, J., Xing, T., 2021. Using t-distributed stochastic neighbor embedding (t-sne) for cluster analysis and spatial zone delineation of groundwater geochemistry data. *Journal of Hydrology* 597, 126146. URL: <https://www.sciencedirect.com/science/article/pii/S0022169421001931>, doi:<https://doi.org/10.1016/j.jhydrol.2021.126146>.
- [108] Liu, M., Wu, Y., Zhang, Q., Wang, F., Li, M., 2016. Synthetic aperture radar target configuration recognition using locality-preserving prop-

erty and the gamma distribution. *IET Radar, Sonar & Navigation* 10, 256–263.

[109] Liu, Q., Liu, L., Wang, Y., Zhang, Z., 2012b. Locally linear embedding based example learning for pan-sharpening, in: *Proceedings of the 21st International Conference on Pattern Recognition (ICPR2012)*, pp. 1928–1931.

[110] Lu, S., Guo, J., Zimmer-Dauphinee, J.R., Nieusma, J.M., Wang, X., vanValkenburgh, P., Wernke, S.A., Huo, Y., 2025. Vision foundation models in remote sensing: A survey. *IEEE Geoscience and Remote Sensing Magazine* , 2–27doi:10.1109/MGRS.2025.3541952.

[111] Lu, X., Zhang, W., Huang, J., 2020. Exploiting embedding manifold of autoencoders for hyperspectral anomaly detection. *IEEE Transactions on Geoscience and Remote Sensing* 58, 1527–1537. doi:10.1109/TGRS.2019.2944419.

[112] Luo, F., Huang, H., Duan, Y., Liu, J., Liao, Y., 2017. Local geometric structure feature for dimensionality reduction of hyperspectral imagery. *Remote Sensing* 9, 790.

[113] Luo, F., Zhang, L., Du, B., Zhang, L., 2020. Dimensionality reduction with enhanced hybrid-graph discriminant learning for hyperspectral image classification. *IEEE Transactions on Geoscience and Remote Sensing* 58, 5336–5353. doi:10.1109/TGRS.2020.2963848.

[114] Luo, G., Chen, G., Tian, L., Qin, K., Qian, S.E., 2016. Minimum noise fraction versus principal component analysis as a preprocessing step for hyperspectral imagery denoising. *Canadian Journal of Remote Sensing* 42, 106–116.

[115] Luo, Y., Liu, R., Zhu, Y., 2008. Fusion of remote sensing image base on the PCA+ATROUS wavelet transform. *International Society for Photogrammetry and Remote Sensing* 37.

[116] Lyzenga, D.R., 1978. Passive remote sensing techniques for mapping water depth and bottom features. *Applied optics* 17, 379–383.

[117] Ma, D., Yuan, Y., Wang, Q., 2018. Hyperspectral anomaly detection via discriminative feature learning with multiple-dictionary sparse

representation. *Remote Sensing* 10. URL: <https://www.mdpi.com/2072-4292/10/5/745>, doi:10.3390/rs10050745.

- [118] Mañas, O., Lacoste, A., Giró-i Nieto, X., Vazquez, D., Rodríguez, P., 2021. Seasonal contrast: Unsupervised pre-training from uncurated remote sensing data, in: Proceedings of the IEEE/CVF International Conference on Computer Vision (ICCV), pp. 9414–9423.
- [119] Van der Maaten, L., Hinton, G., 2008. Visualizing data using t-SNE. *Journal of machine learning research* 9.
- [120] Mahecha, M.D., Gans, F., Sippel, S., Donges, J.F., Kaminski, T., Metzger, S., Migliavacca, M., Papale, D., Rammig, A., Zscheischler, J., 2017. Detecting impacts of extreme events with ecological in situ monitoring networks. *Biogeosciences* 14, 4255–4277. URL: <https://bg.copernicus.org/articles/14/4255/2017/>, doi:10.5194/bg-14-4255-2017.
- [121] Manzanera, J.A., García-Abril, A., Cristina Pascual, R.T., Martín-Fernández, S., Tokola, T., Valbuena, R., 2016. Fusion of airborne LiDAR and multispectral sensors reveals synergic capabilities in forest structure characterization. *GIScience & Remote Sensing* 53, 723–738. URL: <https://doi.org/10.1080/15481603.2016.1231605>, doi:10.1080/15481603.2016.1231605, arXiv:<https://doi.org/10.1080/15481603.2016.1231605>.
- [122] noz Marí, J.M., Izquierdo-Verdiguier, E., Campos-Taberner, M., Pérez-Suay, A., Gómez-Chova, L., Mateo-García, G., Ruescas, A.B., Laparra, V., Padrón, J.A., Amorós, J., Camps-Valls, G., 2017. Hyperlabelme: a web platform for benchmarking remote sensing image classifiers. URL: <http://hyperlabelme.uv.es/>, doi:<https://doi.org/10.1109/MGRS.2017.2762476>. v1.0.
- [123] Marsocci, V., Jia, Y., Bellier, G.L., Kerekes, D., Zeng, L., Hafner, S., Gerard, S., Brune, E., Yadav, R., Shibli, A., Fang, H., Ban, Y., Vergauwen, M., Audebert, N., Nascetti, A., 2025. PANGAEA: A global and inclusive benchmark for geospatial foundation models. URL: <https://arxiv.org/abs/2412.04204>, arXiv:2412.04204.

- [124] Maxwell, A.E., Warner, T.A., Fang, F., 2018. Implementation of machine-learning classification in remote sensing: An applied review. *International journal of remote sensing* 39, 2784–2817.
- [125] McInnes, L., Healy, J., Melville, J., 2018. UMAP: Uniform manifold approximation and projection for dimension reduction. *arXiv preprint arXiv:1802.03426* .
- [126] Micchelli, C.A., Xu, Y., Zhang, H., 2006. Universal kernels. *Journal of Machine Learning Research* 7.
- [127] Najim, S.A., Ahmed, B.Y., 2023. Insightful visualization of remote sensing images. *IEEE Geoscience and Remote Sensing Letters* 20, 1–4. doi:10.1109/LGRS.2022.3228874.
- [128] Nalepa, J., Myller, M., Kawulok, M., 2019. Training- and test-time data augmentation for hyperspectral image segmentation. *IEEE Geoscience and Remote Sensing Letters* PP, 1–5. doi:10.1109/LGRS.2019.2921011.
- [129] Nanga, S., Bawah, A.T., Acquaye, B.A., Billa, M.I., Baeta, F.D., Odai, N.A., Obeng, S.K., Nsiah, A.D., 2021. Review of dimension reduction methods. *Journal of Data Analysis and Information Processing* 9, 189–231.
- [130] Nielsen, A.A., 2010. Kernel maximum autocorrelation factor and minimum noise fraction transformations. *IEEE Transactions on Image Processing* 20, 612–624.
- [131] Niu, Y., Wang, B., 2016. Hyperspectral anomaly detection based on low-rank representation and learned dictionary. *Remote Sensing* 8. URL: <https://www.mdpi.com/2072-4292/8/4/289>.
- [132] Payandeh, A., Baghaei, K.T., Fayyazsanavi, P., Ramezani, S.B., Chen, Z., Rahimi, S., 2023. Deep representation learning: Fundamentals, technologies, applications, and open challenges. *IEEE Access* 11, 137621–137659. doi:10.1109/ACCESS.2023.3335196.
- [133] Pellicer-Valero, O.J., Aybar, C., Valls, G.C., 2025. Video compression for spatiotemporal Earth system data. *arXiv preprint arXiv:2506.19656* .

- [134] Peng, J., Sun, W., Li, H.C., Li, W., Meng, X., Ge, C., Du, Q., 2022. Low-rank and sparse representation for hyperspectral image processing: A review. *IEEE Geoscience and Remote Sensing Magazine* 10, 10–43. doi:10.1109/MGRS.2021.3075491.
- [135] Penna, B., Tillo, T., Magli, E., Olmo, G., 2006. Progressive 3-D coding of hyperspectral images based on JPEG2000. *IEEE Geoscience and Remote Sensing Letters* 3, 125–129.
- [136] Penna, B., Tillo, T., Magli, E., Olmo, G., 2007. Transform coding techniques for lossy hyperspectral data compression. *IEEE Transactions on Geoscience and Remote Sensing* 45, 1408–1421.
- [137] Prudente, V.H.R., Martins, V.S., Vieira, D.C., e Silva, N.R.d.F., Adami, M., Sanches, I.D., 2020. Limitations of cloud cover for optical remote sensing of agricultural areas across South America. *Remote Sensing Applications: Society and Environment* 20, 100414.
- [138] Qiao, T., Ren, J., Wang, Z., Zabalza, J., Sun, M., Zhao, H., Li, S., Benediktsson, J.A., Dai, Q., Marshall, S., 2016. Effective denoising and classification of hyperspectral images using curvelet transform and singular spectrum analysis. *IEEE Transactions on Geoscience and Remote Sensing* 55, 119–133.
- [139] Qin, Z., Zeng, Q., Zong, Y., Xu, F., 2021. Image inpainting based on deep learning: A review. *Displays* 69, 102028.
- [140] Qu, Y., Qi, H., 2018. uDAS: An untied denoising autoencoder with sparsity for spectral unmixing. *IEEE Transactions on Geoscience and Remote Sensing* 57, 1698–1712.
- [141] Radford, A., Kim, J.W., Hallacy, C., Ramesh, A., Goh, G., Agarwal, S., Sastry, G., Askell, A., Mishkin, P., Clark, J., et al., 2021. Learning transferable visual models from natural language supervision, in: International conference on machine learning, PMLR. pp. 8748–8763.
- [142] Ramos-Pollan, R., Kalaitzis, F., Selvam, K.P., 2024. Uncertainty and generalizability in foundation models for Earth observation. URL: <https://arxiv.org/abs/2409.08744>, arXiv:2409.08744.

- [143] Rasti, B., Chang, Y., Dalsasso, E., Denis, L., Ghamisi, P., 2021. Image restoration for remote sensing: Overview and toolbox. *IEEE Geoscience and Remote Sensing Magazine* 10, 201–230.
- [144] Rasti, B., Hong, D., Hang, R., Ghamisi, P., Kang, X., Chanussot, J., Benediktsson, J.A., 2020. Feature extraction for hyperspectral imagery: The evolution from shallow to deep: Overview and toolbox. *IEEE Geoscience and Remote Sensing Magazine* 8, 60–88. doi:10.1109/MGRS.2020.2979764.
- [145] Reichstein, M., Camps-Valls, G., Stevens, B., Jung, M., Denzler, J., Carvalhais, N., Prabhat, F., 2019. Deep learning and process understanding for data-driven Earth system science. *Nature* 566, 195–204.
- [146] Rivera-Caicedo, J.P., Verrelst, J., Muñoz-Marí, J., Camps-Valls, G., Moreno, J., 2017. Hyperspectral dimensionality reduction for biophysical variable statistical retrieval. *ISPRS journal of photogrammetry and remote sensing* 132, 88–101.
- [147] Rosipal, R., Trejo, L.J., 2001. Kernel partial least squares regression in reproducing kernel Hilbert space. *Journal of Machine Learning Research* 2, 97–123.
- [148] Rumelhart, D.E., Hinton, G.E., Williams, R.J., 1986. Learning representations by back-propagating errors. *Nature* 323, 533–536.
- [149] Runge, J., Petoukhov, V., Donges, J.F., Hlinka, J., Jajcay, N., Vejmelka, M., Hartman, D., Marwan, N., Paluš, M., Kurths, J., et al., 2015. Identifying causal gateways and mediators in complex spatio-temporal systems. *Nature Communications* 6.
- [150] Rußwurm, M., Körner, M., 2020. Self-attention for raw optical satellite time series classification. *ISPRS journal of photogrammetry and remote sensing* 169, 421–435.
- [151] Saeed, N., Nam, H., Haq, M.I.U., Muhammad Saqib, D.B., 2018. A survey on multidimensional scaling. *ACM Computing Surveys (CSUR)* 51, 1–25.

[152] Saul, L.K., Roweis, S.T., 2000. An introduction to locally linear embedding. unpublished. Available at: <http://www.cs.toronto.edu/~roweis/lle/publications.html> .

[153] Schölkopf, B., Smola, A., Müller, K.R., 1997. Kernel principal component analysis, in: International conference on artificial neural networks, Springer. pp. 583–588.

[154] Serra-Sagristà, J., Aulí-Llinàs, F., 2008. Remote sensing data compression, in: Computational Intelligence for Remote Sensing. Springer, pp. 27–61.

[155] Shah, V.P., Younan, N.H., King, R.L., 2008. An efficient pancharpening method via a combined adaptive pca approach and contourlets. *IEEE Transactions on Geoscience and Remote Sensing* 46, 1323–1335. doi:10.1109/TGRS.2008.916211.

[156] Shao, Z., Zhang, L., Wang, L., 2017. Stacked sparse autoencoder modeling using the synergy of airborne LiDAR and satellite optical and SAR data to map forest above-ground biomass. *IEEE Journal of Selected Topics in Applied Earth Observations and Remote Sensing* 10, 5569–5582. doi:10.1109/JSTARS.2017.2748341.

[157] Shen, H., Li, H., Qian, Y., Zhang, L., Yuan, Q., 2014. An effective thin cloud removal procedure for visible remote sensing images. *ISPRS Journal of Photogrammetry and Remote Sensing* 96, 224–235.

[158] Shen, H., Li, X., Cheng, Q., Zeng, C., Yang, G., Li, H., Zhang, L., 2015a. Missing information reconstruction of remote sensing data: A technical review. *IEEE Geoscience and Remote Sensing Magazine* 3, 61–85.

[159] Shen, H., Li, X., Cheng, Q., Zeng, C., Yang, G., Li, H., Zhang, L., 2015b. Missing information reconstruction of remote sensing data: A technical review. *IEEE Geoscience and Remote Sensing Magazine* 3, 61–85. doi:10.1109/MGRS.2015.2441912.

[160] Shi, J., Wu, T., Kai Qin, A., Lei, Y., Jeon, G., 2024. Self-guided autoencoders for unsupervised change detection in heterogeneous remote sensing images. *IEEE Transactions on Artificial Intelligence* 5, 2458–2471. doi:10.1109/TAI.2024.3357667.

[161] Shurmer, I., Marchese, F., Morales-Santiago, J.M., Emanuelli, P.P., 2018. Sentinels optical communications payload (ocp) operations: From test to in-flight experience, in: 2018 SpaceOps Conference, p. 2654.

[162] Sirjacobs, D., Alvera-Azcárate, A., Barth, A., Lacroix, G., Park, Y., Nechad, B., Ruddick, K., Beckers, J.M., 2011. Cloud filling of ocean colour and sea surface temperature remote sensing products over the Southern North Sea by the Data Interpolating Empirical Orthogonal Functions methodology. *Journal of Sea Research* 65, 114–130.

[163] Skodras, A., Christopoulos, C., Ebrahimi, T., 2001. The JPEG 2000 still image compression standard. *IEEE Signal processing magazine* 18, 36–58.

[164] Song, Q., Xu, F., Zhu, X.X., Jin, Y.Q., 2021. Learning to generate SAR images with adversarial autoencoder. *IEEE Transactions on Geoscience and Remote Sensing* 60, 1–15.

[165] Song, W., Wang, L., Liu, P., Choo, K.K.R., 2019. Improved t-SNE based manifold dimensional reduction for remote sensing data processing. *Multimedia Tools and Applications* 78. doi:10.1007/s11042-018-5715-0.

[166] Sun, W., Liu, C., Li, J., Lai, Y.M., Li, W., 2014. Low-rank and sparse matrix decomposition-based anomaly detection for hyperspectral imagery. *Journal of Applied Remote Sensing* 8, 083641. URL: <https://doi.org/10.1117/1.JRS.8.083641>, doi:10.1117/1.JRS.8.083641.

[167] Szwagier, T., Pennec, X., 2024. The curse of isotropy: From principal components to principal subspaces URL: <https://arxiv.org/abs/2307.15348>, arXiv:2307.15348.

[168] Szwarcman, D., Roy, S., Fraccaro, P., Gíslason, P.E., Blumenstiel, B., Ghosal, R., de Oliveira, P.H., de Sousa Almeida, J.L., Sedona, R., Kang, Y., Chakraborty, S., Wang, S., Gomes, C., Kumar, A., Truong, M., Godwin, D., Lee, H., Hsu, C.Y., Asanjan, A.A., Mujeci, B., Shidham, D., Keenan, T., Arevalo, P., Li, W., Alemohammad, H., Olofsson,

P., Hain, C., Kennedy, R., Zadrozny, B., Bell, D., Cavallaro, G., Watson, C., Maskey, M., Ramachandran, R., Moreno, J.B., 2025. Prithvi-eo-2.0: A versatile multi-temporal foundation model for Earth observation applications. URL: <https://arxiv.org/abs/2412.02732>, arXiv:2412.02732.

[169] Tan, K., Hou, Z., Ma, D., Chen, Y., Du, Q., 2019. Anomaly detection in hyperspectral imagery based on low-rank representation incorporating a spatial constraint. *Remote Sensing* 11. URL: <https://www.mdpi.com/2072-4292/11/13/1578>.

[170] Tasdemir, K., Merényi, E., 2009. Exploiting data topology in visualization and clustering of self-organizing maps. *IEEE Transactions on Neural Networks* 20, 549–562.

[171] Touati, R., Mignotte, M., Dahmane, M., 2018. Change detection in heterogeneous remote sensing images based on an imaging modality-invariant MDS representation, in: 2018 25th IEEE International Conference on Image Processing (ICIP), pp. 3998–4002. doi:10.1109/ICIP.2018.8451184.

[172] Tsakiris, M.C., Vidal, R., 2018. Dual principal component pursuit. *Journal of Machine Learning Research* 19, 1–50.

[173] Tseng, G., Cartuyvels, R., Zvonkov, I., Purohit, M., Rolnick, D., Kerner, H., 2024. Lightweight, pre-trained transformers for remote sensing timeseries. URL: <https://arxiv.org/abs/2304.14065>, arXiv:2304.14065.

[174] Tuia, D., Roscher, R., Wegner, J., Jacobs, N., Zhu, X., Camps-Valls, G., 2021. Towards a Collective Agenda on AI for Earth Science Data Analysis. *IEEE Geoscience and Remote Sensing Magazine* 9, 88–104. doi:<https://doi.org/10.1109/MGRS.2020.3043504>.

[175] Tuia, D., Volpi, M., Trolliet, M., Camps-Valls, G., 2014. Semisupervised manifold alignment of multimodal remote sensing images. *IEEE Transactions on Geoscience and Remote Sensing* 52, 7708–7720.

[176] Vaddi, R., Manoharan, P., 2020. Probabilistic PCA based hyper spectral image classification for remote sensing applications, in: Intelligent

Systems Design and Applications: 18th International Conference on Intelligent Systems Design and Applications (ISDA 2018) held in Vellore, India, December 6-8, 2018, Volume 2, Springer. pp. 863–869.

- [177] Van Der Maaten, L., Postma, E.O., Van Den Herik, H.J., et al., 2009. Dimensionality reduction: A comparative review. *Journal of machine learning research* 10, 13.
- [178] Van Westen, C., 2000. Remote sensing for natural disaster management. *International archives of photogrammetry and remote sensing* 33, 1609–1617.
- [179] Vanonckelen, S., Lhermitte, S., Van Rompaey, A., 2013. The effect of atmospheric and topographic correction methods on land cover classification accuracy. *International Journal of Applied Earth Observation and Geoinformation* 24, 9–21.
- [180] Varando, G., Fernández-Torres, M.Á., Muñoz-Marí, J., Camps-Valls, G., 2022. Learning causal representations with Granger PCA, in: UAI 2022 Workshop on Causal Representation Learning.
- [181] Vautard, R., Ghil, M., 1989. Singular spectrum analysis in nonlinear dynamics, with applications to paleoclimatic time series. *Physica D: Nonlinear Phenomena* 35, 395–424.
- [182] Wald, L., Ranchin, T., Mangolini, M., 1997. Fusion of satellite images of different spatial resolutions: Assessing the quality of resulting images. *Photogrammetric engineering and remote sensing* 63, 691–699.
- [183] Waldmann, L., Shah, A., Wang, Y., Lehmann, N., Stewart, A.J., Xiong, Z., Zhu, X.X., Bauer, S., Chuang, J., 2025. Panopticon: Advancing any-sensor foundation models for Earth observation. URL: <https://arxiv.org/abs/2503.10845>, arXiv:2503.10845.
- [184] Wang, G., Garcia, D., Liu, Y., De Jeu, R., Dolman, A.J., 2012. A three-dimensional gap filling method for large geophysical datasets: Application to global satellite soil moisture observations. *Environmental Modelling & Software* 30, 139–142.

- [185] Wang, J., Chang, C.I., 2006. Independent component analysis-based dimensionality reduction with applications in hyperspectral image analysis. *IEEE transactions on Geoscience and Remote Sensing* 44, 1586–1600.
- [186] Wang, M., Hong, D., Han, Z., Li, J., Yao, J., Gao, L., Zhang, B., Chanussot, J., 2023. Tensor decompositions for hyperspectral data processing in remote sensing: A comprehensive review. *IEEE Geoscience and Remote Sensing Magazine* 11, 26–72.
- [187] Wang, S., Wang, X., Zhang, L., Zhong, Y., 2022a. Auto-AD: Autonomous hyperspectral anomaly detection network based on fully convolutional autoencoder. *IEEE Transactions on Geoscience and Remote Sensing* 60, 1–15. doi:10.1109/TGRS.2022.3207165.
- [188] Wang, T., Wang, H., Sun, H., 2022b. Adaptive loss function-based autoencoder for hyperspectral anomaly detection. *IEEE Transactions on Image Processing* 31, 2234–2247. doi:10.1109/TIP.2022.3142547.
- [189] Wang, Y., Albrecht, C.M., Braham, N.A.A., Mou, L., Zhu, X.X., 2022c. Self-supervised learning in remote sensing: A review. *IEEE Geoscience and Remote Sensing Magazine* 10, 213–247. doi:10.1109/MGRS.2022.3198244.
- [190] Wang, Y.X., Zhang, Y.J., 2012. Nonnegative matrix factorization: A comprehensive review. *IEEE Transactions on knowledge and data engineering* 25, 1336–1353.
- [191] Wang, Z., Bovik, A.C., 2002. A universal image quality index. *IEEE signal processing letters* 9, 81–84.
- [192] Wang, Z., He, X., Xiao, B., Chen, L., Bi, X., 2024. Rsid-cr: Remote sensing image denoising based on contrastive learning. *IEEE Journal of Selected Topics in Applied Earth Observations and Remote Sensing* 17, 18784–18799. doi:10.1109/JSTARS.2024.3476566.
- [193] Weiss, M., Jacob, F., Duveiller, G., 2020. Remote sensing for agricultural applications: A meta-review. *Remote sensing of environment* 236, 111402.

[194] Wellmann, T., Lausch, A., Andersson, E., Knapp, S., Cortinovis, C., Jache, J., Scheuer, S., Kremer, P., Mascarenhas, A., Kraemer, R., et al., 2020. Remote sensing in urban planning: Contributions towards ecologically sound policies? *Landscape and urban planning* 204, 103921.

[195] Wu, Z., Wang, B., 2024. Transformer-based autoencoder framework for nonlinear hyperspectral anomaly detection. *IEEE Transactions on Geoscience and Remote Sensing* 62, 61469–61481. doi:10.1109/TGRS.2024.3361469.

[196] Xiang, P., Ali, S., Jung, S.K., Zhou, H., 2021. Hyperspectral anomaly detection with guided autoencoder. *IEEE Transactions on Geoscience and Remote Sensing* 60, 1–15. doi:10.1109/TGRS.2021.3057721.

[197] Xiang, S., Liang, Q., 2024. Remote sensing image compression based on high-frequency and low-frequency components. *IEEE Transactions on Geoscience and Remote Sensing* .

[198] Xie, Y., Tao, R., Peng, X., 2019. Spectral constraint adversarial autoencoder for hyperspectral anomaly detection. *Neural Networks* 118, 107–120. doi:10.1016/j.neunet.2019.07.001.

[199] Xing, Y., Wang, M., Yang, S., Jiao, L., 2018. Pan-sharpening via deep metric learning. *ISPRS Journal of Photogrammetry and Remote Sensing* 145, 165–183. URL: <https://www.sciencedirect.com/science/article/pii/S0924271618300212>, doi:<https://doi.org/10.1016/j.isprsjprs.2018.01.016>. deep Learning RS Data.

[200] Xiong, Z., Wang, Y., Zhang, F., Stewart, A.J., Hanna, J., Borth, D., Papoutsis, I., Saux, B.L., Camps-Valls, G., Zhu, X.X., 2024. Neural plasticity-inspired multimodal foundation model for Earth observation. URL: <https://arxiv.org/abs/2403.15356>, arXiv:2403.15356.

[201] Xu, M., Jia, X., Pickering, M., Plaza, A.J., 2016. Cloud removal based on sparse representation via multitemporal dictionary learning. *IEEE Transactions on Geoscience and Remote Sensing* 54, 2998–3006.

[202] Xu, Z., Jiang, W., Geng, J., 2024. Texture-aware causal feature extraction network for multimodal remote sensing data classification. *IEEE Transactions on Geoscience and Remote Sensing* .

[203] Yan, S., Xu, D., Zhang, B., Zhang, H.J., Yang, Q., Lin, S., 2006. Graph embedding and extensions: A general framework for dimensionality reduction. *IEEE Transactions on Pattern Analysis and Machine Intelligence* 29, 40–51.

[204] Yang, S., Wang, M., Jiao, L., 2012. Fusion of multispectral and panchromatic images based on support value transform and adaptive principal component analysis. *Information Fusion* 13, 177–184. URL: <https://www.sciencedirect.com/science/article/pii/S1566253510000898>, doi:<https://doi.org/10.1016/j.inffus.2010.09.003>.

[205] Yang, W., Wang, J., Guo, J., 2013. A novel algorithm for satellite images fusion based on compressed sensing and PCA. *Mathematical Problems in Engineering* 2013, 708985. doi:<https://doi.org/10.1155/2013/708985>.

[206] Yang, X., Liu, W., Liu, W., Tao, D., 2019. A survey on canonical correlation analysis. *IEEE Transactions on Knowledge and Data Engineering* 33, 2349–2368.

[207] Yoshua Bengio, A.C., Vincent, P., 2013. Representation learning: A review and new perspectives. *IEEE Transactions on Pattern Analysis and Machine Intelligence* 35, 1798–1828. doi:[10.1109/TPAMI.2013.50](https://doi.org/10.1109/TPAMI.2013.50).

[208] Yousif, O., Ban, Y., 2013. Improving urban change detection from multitemporal SAR images using PCA-NLM. *IEEE Transactions on Geoscience and Remote Sensing* 51, 2032–2041. doi:[10.1109/TGRS.2013.2245900](https://doi.org/10.1109/TGRS.2013.2245900).

[209] Zhang, B., Zhao, L., Zhang, X., 2020. Three-dimensional convolutional neural network model for tree species classification using airborne hyperspectral images. *Remote Sensing of Environment* 247, 111938.

[210] Zhao, W.X., Zhou, K., Li, J., Tang, T., Wang, X., Hou, Y., Min, Y., Zhang, B., Zhang, J., Dong, Z., Du, Y., Yang, C., Chen, Y., Chen, Z., Jiang, J., Ren, R., Li, Y., Tang, X., Liu, Z., Liu, P., Nie, J.Y., Wen, J.R., 2025. A survey of large language models. URL: <https://arxiv.org/abs/2303.18223>, arXiv:2303.18223.

- [211] Zhu, X.X., Tuia, D., Mou, L., Xia, G.S., Zhang, L., Xu, F., Fraundorfer, F., 2017. Deep learning in remote sensing: A comprehensive review and list of resources. *IEEE Geoscience and Remote Sensing Magazine* 5, 8–36.
- [212] Zhu, X.X., Xiong, Z., Wang, Y., Stewart, A.J., Heidler, K., Wang, Y., Yuan, Z., Dujardin, T., Xu, Q., Shi, Y., 2024. On the foundations of Earth and climate foundation models. URL: <https://arxiv.org/abs/2405.04285>, arXiv:2405.04285.

Appendix A. Supplementary Material

A list of standard Dimensionality Reduction (DR) methods in Remote Sensing (RS) is in Tab. A.5. The dimensionality sources for different RS sensors are in Tab. A.4. We provide two look-up tables that organize our references. Tab. A.6 sorts references for DR in RS by the standard DR methods used to address each challenge, sorted by property preservation. Next, Tab. A.7 organized the references of evaluation metrics for DR in RS by RS task.

Table A.4: **Sources of data dimensionality across common remote-sensing sensors.**

Sensor Type	Dimensionality Sources
Optical / Multispectral/ Hyperspectral	spatial resolution spectral bands temporal revisits
Thermal Infrared Imager	spatial resolution thermal bands temperature sensitivity temporal revisits
Passive Microwave Radiometer	footprint size multiple centre frequencies polarisation temporal coverage
Atmospheric Spectrometer / Sounder	vertical profile levels spectral resolution along-track sampling temporal coverage
SAR / Radar	frequency band polarisation phase/coherence incidence angle temporal stacks
LiDAR	point density 3D geometry multiple returns waveform samples

Table A.5: Standard DR methods for RS with abbreviations and references.

AE	Autoencoder	[12]
CCA	Canonical Correlation Analysis	[206]
DCT	Discrete Cosine Transform	[2]
CLIP	Contrastive Language Image Pre-training	[141]
DCuT	Discrete Curvelet Transform	[27]
DFT	Discrete Fourier Transform	[49]
DL	Dictionary Learning	[93]
DWT	Discrete Wavelet Transform	[18]
EOF	Empirical Orthogonal Functions	[67]
GDA	Generalized Discriminant Analysis	[14]
ICA	Independent Component Analysis	[81]
Isomap	Isometric Feature Mapping	[9]
kCCA	Kernel Canonical Correlation Analysis	[3]
kMNF	Kernel Maximum Noise Fraction	[130]
kPCA	Kernel Principal component analysis	[153]
kPLS	Kernel Partial Least Squares	[147]
LDA	Linear Discriminant Analysis	[11]
LLE	Locally Linear Embedding	[152]
MA	Manifold Alignment	[66]
MDS	Multidimensional Scaling	[151]
MFA	Marginal Fisher Analysis	[203]
MNF	Maximum Noise Fraction	[61]
NMF	Non-negative Matrix Factorization	[190]
OSP	Orthogonal Subspace Projection	[69]
PCA	Principal Component Analysis	[72]
PLS	Partial Least Squares	[65]
POD	Proper Orthogonal Decomposition	[31]
SOM	Self-organizing Maps	[92]
SSA	Singular Spectrum Analysis	[181]
TD	Tensor Decomposition	[186]
t-SNE	t-Distributed Stochastic Neighbor Embedding	[119]
VAE	Variational Autoencoder	[88]

Table A.6: **We align DR methods with their corresponding RS tasks.** Each row represents a DR method, each column an RS task, and each cell lists representative papers where the method has been applied to the task. For clarity, papers using variants, combinations, or improvements of a DR method are listed under the base method they extend.

Signal and Structure Preserving					
	Compression	Data Cleaning	Fusion	Visualization	Anomaly Detection
CuT			[155]		[138]
DFT	[15]				[17]
DWT	[15, 82, 163, 135, 154, 55, 46, 197]	[33]	[115]	[45]	[20, 86, 55, 136]
Linear Variance and Reconstruction Preserving					
	Compression	Data Cleaning	Fusion	Visualization	Anomaly Detection
CCA			[121]		[146]
DL		[201, 102]		[169, 131, 44, 117, 166, 35]	
LDA					[101, 100, 112, 113]
MNF		[114]			[146]
OSP					[69]
PCA	[82, 45, 136, 154, 46]	[33, 162, 114, 47, 83]	[115, 205, 155, 204, 103]	[26, 71, 13, 21, 149, 38]	[47, 79, 208, 51, 120, 52, 45]
PLS		[184]			[146]
POT	[15, 55]				[55]
TD	[46, 86]				[86]
Nonlinear Variance and Reconstruction Preserving					
	Compression	Data Cleaning	Fusion	Visualization	Anomaly Detection
AE		[139, 140]	[75, 105, 74, 199, 58, 156]	[62, 77]	[198, 111, 195, 50, 76, 196, 187, 160]
kPCA					[63]
Distribution Preserving					
	Compression	Data Cleaning	Fusion	Visualization	Anomaly Detection
ICA		[82, 185]			[52]
VAE		[42]			[94, 68]
Geometry & Topology Preserving					
	Compression	Data Cleaning	Fusion	Visualization	Anomaly Detection
Isomap				[8]	[8]
LE			[40, 103]		
LLE			[109]	[8]	[8]
MA			[175]		[175]
MDS				[171]	
SOM				[170, 127]	
t-SNE				[165, 209, 150]	

Table A.7: The metrics used by the articles surveyed for dimensionality reduction in remote sensing.

	Compression	Denoising	Fusion	Visualization	Anom. Dect.	Predictions
CC	[86, 46]	[162, 184, 158, 102]	[32, 115, 204, 104, 205, 75, 121, 156, 74]	[70, 21, 127, 77]	[45]	[121, 164]
MSE	[82, 46]	[162, 184, 83, 157, 201, 102, 43, 47]	[204, 75, 156, 199, 74]	[127]	[35]	[136, 17, 55, 156, 146]
ACC		[47]	[104, 175, 40, 58, 103]		[171, 160]	[128, 176, 20, 138, 101, 112, 100, 113, 108, 90, 164, 136, 97, 86, 103, 40, 175]
VIS	[15, 197]	[33, 162, 184, 43, 140, 102, 47, 42]	[205, 155, 204, 75, 74, 104, 199, 175, 107]	[165, 209, 13, 21, 77]	[63, 169, 131, 44, 117, 35, 198, 111, 195, 50, 76, 196, 187, 188, 208, 171, 160, 120, 51]	[138, 101, 112, 8, 100, 113, 90, 164, 69, 97]
CT	[86, 46, 82, 196]	[140, 102]	[175, 74]		[79, 50, 76, 160]	[8, 146, 100]
κ			[175, 40, 103, 58]		[160]	[128, 176, 100, 136, 97, 103, 40, 175]
SAD/ SAM	[86, 46]	[158, 201, 140]	[155, 204, 104, 75, 199, 106, 74]			
SNR	[15, 135, 136, 45, 86, 55, 46]	[162, 33]				
PSNR	[135, 136, 46]	[158, 201, 102, 196, 42]				
BR	[82, 135, 136, 45, 86, 55, 46]					
RD	[135, 45, 55, 197]					
ERGAS			[155, 204, 75, 199, 106, 74, 199]			
Q			[155, 204, 104, 75, 199, 74]			
AUC					[79, 63, 169, 131, 44, 117, 35, 198, 111, 195, 50, 76, 196, 188, 187, 208, 160, 52, 45]	
R^2						[90, 146, 17]